

CONTROL TECHNIQUES IN DYNAMIC COMMUNICATION NETWORKS

By

SANKRITH SUBRAMANIAN

A DISSERTATION PRESENTED TO THE GRADUATE SCHOOL
OF THE UNIVERSITY OF FLORIDA IN PARTIAL FULFILLMENT
OF THE REQUIREMENTS FOR THE DEGREE OF
DOCTOR OF PHILOSOPHY

UNIVERSITY OF FLORIDA

2012

© 2012 Sankrith Subramanian

To my mother and father

ACKNOWLEDGMENTS

I express my most sincere appreciation to my supervisory committee chair and mentor, Dr. Warren E. Dixon. I thank him for the education, advice, and the encouragement that he had provided me with during the course of my study at the University of Florida. I also thank Dr. John M. Shea for lending his knowledge and support, and providing technical guidance. It is a great privilege to have worked with such far-thinking and inspirational individuals. All that I have learnt and accomplished would not have been possible without their dedication.

I also extend my appreciation to Dr. Jess W. Curtis and Dr. Eduardo L. Pasilliao for their support and collaborative efforts, along with my colleagues at University of Florida for encouraging some thought-provoking analytical discussions.

Most importantly, I would like to express my deepest appreciation to my parents P. R. Subramanian and Indhumathi Subramanian, and my sister Shilpa Subramanian. Their love, understanding, patience and personal sacrifice made this dissertation possible.

TABLE OF CONTENTS

	<u>page</u>
ACKNOWLEDGMENTS	4
LIST OF TABLES	7
LIST OF FIGURES	8
ABSTRACT	10
CHAPTER	
1 INTRODUCTION	12
2 POWER CONTROL FOR CELLULAR COMMUNICATIONS WITH TIME-VARYING CHANNEL UNCERTAINTIES	19
2.1 Network Model and Properties	20
2.2 Linear Prediction	22
2.3 Control Development	25
2.3.1 Control Objective	25
2.3.2 Closed-Loop Error System	25
2.4 Stability Analysis	26
2.5 Simulation Results	28
2.6 Power-Control Mechanism	34
3 THROUGHPUT MAXIMIZATION IN CSMA NETWORKS	40
3.1 Throughput Maximization in CSMA Networks with Collisions	40
3.1.1 Network Model	40
3.1.2 CSMA Markov Chain	42
3.1.3 Throughput Maximization	44
3.1.4 Simulation Results	48
3.2 Throughput Maximization in CSMA Networks with Collisions and Hidden Terminals	53
3.2.1 Network Model	53
3.2.2 CSMA Markov Chain	54
3.2.3 Throughput Maximization	57
3.2.4 Simulation Results	59
4 CONGESTION CONTROL FOR DIFFERENTIATED-SERVICES NETWORKS WITH ARRIVAL-RATE DELAYS	62
4.1 Queuing System Model	62
4.2 Premium Service	64
4.2.1 Control Design	65
4.2.2 Stability Analysis	66

4.3	Ordinary Service	69
4.3.1	Stability Analysis	70
4.4	Simulation Results	72
5	CONCLUSION	77
5.1	Summary of Results	77
5.2	Recommendations for Future Work	78
APPENDIX		
A	ESTIMATION OF RANDOM PROCESSES	79
A-1	General MMSE based estimation theory	79
A-2	Gaussian Case	80
B	ORTHOGONALITY CONDITION	82
C	PROOF OF $P \geq 0$	84
	REFERENCES	86
	BIOGRAPHICAL SKETCH	94

LIST OF TABLES

<u>Table</u>	<u>page</u>
2-1 Comparison against various prediction window sizes.	33
2-2 Percentage of sample times experiencing outage for different number of users in the cell of interest. The control gain k_p is tuned for the system based on the number of users, and $k_e = 1.3 \times 10^{-4}$. The prediction window sizes are selected based on the condition $\det Z \geq \zeta$ (refer to Table 2-1 for the best window size selection).	34
2-3 Percentage of sample times experiencing outage for unquantized, 2-bit and 3-bit power-control commands.	38
3-1 Optimal values of the mean transmission rates for a 2-link collision network for various values of sensing delays. The optimum values of the mean transmission rates are the solution to the constrained problem defined in (3-9), (3-14), and (3-15).	50
3-2 Optimal values of the mean transmission rates for a 3-link collision network for various values of sensing delays. The optimum values of the mean transmission rates are the solution to the constrained problem defined in (3-9), (3-14), and (3-15).	51
3-3 Average number of collisions for a 2-link and 3-link collision networks for various values of sensing delays. The optimum values of the mean transmission rates are the solution to the constrained problem defined in (3-9), (3-14), and (3-15).	52
3-4 Optimal values of the mean transmission rates for a 3-link collision network with hidden terminals (refer to Fig. 3-7) for various values of sensing delays. The optimum values of the mean transmission rates are the solution to the constrained problem defined in (3-21)-(3-23).	60

LIST OF FIGURES

<u>Figure</u>	<u>page</u>
2-1 Error, channel gain, and power plot of a MT with maximum Doppler frequency 1.35 Hz.	30
2-2 Prediction error of the MT with maximum Doppler frequency 1.35 Hz.	31
2-3 Error, channel gain, and power plot of a MT with maximum Doppler frequency 31.60 Hz.	31
2-4 Prediction error of the MT with maximum Doppler frequency 31.60Hz.	32
2-5 Uplink power-control mechanism.	35
2-6 Probability density function of the SINR errors of all the MTs operating at high (> 25 Hz) maximum Doppler frequencies	36
2-7 Comparison against Song’s power control algorithm.	39
3-1 A n -link network scenario and conflict graph.	41
3-2 CSMA Markov chain for a 2-link scenario with collision states.	43
3-3 Mean transmission rates of nodes 1, 2, and 3 transmitting to the same node 4. All nodes are in the sensing region. The online algorithm of (3–9) is used with $T = 100$ ms, $K = 5$, and $\delta T_s = 0.001$ ms.	48
3-4 Queue lengths of nodes 1 and 2 transmitting to the same node 3. The optimum values of the mean transmission rates are the solution to the constrained problem defined in (3–9), (3–14), and (3–15). All nodes are in the sensing region. $\delta T_s = 0.01$ ms, $R_1 = 6.05$ dataunits/ms, $R_2 = 6.49$ dataunits/ms, $\lambda_1 = 0.16$ dataunits/ms, $\lambda_2 = 0.2$ dataunits/ms.	51
3-5 Queue lengths of nodes 1, 2, and 3 transmitting to the same node 4. The optimum values of the mean transmission rates are the solution to the constrained problem defined in (3–9), (3–14), and (3–15). All nodes are in the sensing region. $\delta T_s = 0.01$ ms, $R_1 = 6.54$ dataunits/ms, $R_2 = 10.19$ dataunits/ms, $R_3 = 11.49$ dataunits/ms, $\lambda_1 = 0.02$ dataunits/ms, $\lambda_2 = 0.05$ dataunits/ms, $\lambda_3 = 0.05$ dataunits/ms.	52
3-6 An $(n + k)$ -link network scenario and conflict graph.	54
3-7 CSMA Markov chain with collision states for a 3-link network scenario with hidden terminals.	55

3-8	Queue lengths of nodes 1, 2, and 4 transmitting to the same node 3. The optimum values of the mean transmission rates are the solution to the constrained problem defined in (3–21)-(3–23). All nodes are in the sensing region, and $\delta T_s = 0.01$ ms, $R_1 = 3.78$ dataunits/ms, $R_2 = 3.58$ dataunits/ms, $R_3 = 2.23$ dataunits/ms, $\lambda_1 = 0.02$ dataunits/ms, $\lambda_2 = 0.05$ dataunits/ms, $\lambda_3 = 0.05$ dataunits/ms.	61
4-1	Schematic of a DiffServ Queueing System.	63
4-2	Ensemble average queue length and service rates for Premium Service without arrival-rate delays.	74
4-3	Ensemble average queue length and average arrival rates for Ordinary Service without arrival-rate delays.	74
4-4	Ensemble average queue length and service rates for Premium Service with average arrival-rate delay.	75
4-5	Ensemble average queue length and average arrival-rate for Ordinary Service with average arrival-rate delay.	76

Abstract of Dissertation Presented to the Graduate School
of the University of Florida in Partial Fulfillment of the
Requirements for the Degree of Doctor of Philosophy

CONTROL TECHNIQUES IN DYNAMIC COMMUNICATION NETWORKS

By

Sankrith Subramanian

December 2012

Chair: Warren E. Dixon

Cochair: John M. Shea

Major: Electrical and Computer Engineering

Power control in the Physical Layer of a communication network is used to ensure that each link achieves its target signal-to-interference-plus-noise ratio (SINR) to effect communication in the reverse link (uplink) of a wireless cellular communication network. In cellular systems using direct-sequence code-division multiple access (CDMA), the SINR depends inversely on the power assigned to the other users in the system, creating a nonlinear control problem. Due to the spreading of bands in CDMA based cellular communication networks, the interference in the system is mitigated. The nonlinearity now arises by the uncertain random phenomena across the radio link, causing detrimental effects to the signal power that is desired at the base station. Mobility of the terminals, along with associated random shadowing and multi-path fading present in the radio link, results in uncertainty in the channel parameters. To quantify these effects, a nonlinear MIMO discrete differential equation is built with the SINR of the radio-link as the state to analyze the behavior of the network. Controllers are designed based on analysis of this networked system, and power updates are obtained from the control law. Analysis is also provided to examine how mobility and the desired SINR regulation range affects the choice of channel update times. Realistic wireless network mobility models are used for simulation and the power control algorithm formulated from the control development is verified on this mobility model for acceptable communication.

In the Medium Access Control (MAC) layer of a wireless network that uses Carrier Sense Multiple Access (CSMA), the performance is limited by collisions that occur because of carrier sensing delays associated with propagation and the sensing electronics, and hidden terminals in the network. A continuous-time Markov model is used to analyze and optimize the performance of a system using CSMA with collisions caused by sensing delays. The throughput of the network is quantified using the stationary distribution of the Markov model. An online algorithm is developed for the unconstrained throughput maximization problem. Further, a constrained problem is formulated and solved using a numerical algorithm. Simulations are provided to analyze and validate the solution to the unconstrained and constrained optimization problems.

Network traffic in the transport layer of end-to-end congestion networks plays a vital role in affecting the throughput in the MAC layer. Common queue length management techniques on nodes in such networks focus on servicing the packets based on their Quality of Service (QoS) requirements (e.g., Differentiated-Services, or DiffServ, networks). In Chapter 4, continuous control strategies are suggested for a DiffServ network to track the desired ensemble average queue length level in the Premium and Ordinary Service buffers specified by the network operator. A Lyapunov-based stability analysis is provided to illustrate global asymptotic tracking of the ensemble average queue length of the Premium Service buffer. In addition, arrival rate delays due to propagation and processing that affects the control input of the Ordinary Service buffer is addressed, and a Lyapunov-based stability analysis is provided to illustrate global asymptotic tracking of the ensemble average queue length of this service. Simulations demonstrate the performance and feasibility of the controller, along with showing global asymptotic tracking of the queue lengths in the Premium Service and Ordinary Service buffers.

CHAPTER 1 INTRODUCTION

The field of communications faces a multitude of challenges while providing Quality of Service (QoS) for a broad class of applications. For instance, the mobility of nodes in a wireless network cause random shifts in the doppler frequencies of the signal that is being transmitted the node to a receiver node. In addition, due to the presence of obstacles in the path, scattering of the signal takes place, and the received signal is the summation of these random phase-shifted multi-path signals. This phenomena is commonly known as multi-path fading, and various models are developed in the literature to characterize the phenomena. Various techniques such as power control, adaptive modulation and coding, symbol mapping diversity, time/space diversity reception etc. are used to mitigate multi-path fading.

Various transmitter power-control methods have been developed to deliver a desired quality of service (QoS) in wireless networks [1–20]. Early work on power control using a centralized approach was investigated in [1], which introduced the concept of signal-to-interference (SIR)-balancing, where it is desired that all receivers achieve the same SIR. In [2], the optimal solution to the SIR-balancing problem is derived by reformulating the problem as an eigenvalue/eigenvector problem and invoking the Perron-Frobenius theorem. Methods were developed to reduce co-channel interference for a given channel allocation using transmitter power control in [3] and [5]. In [5], the performance of optimum transmit-power algorithms are analyzed in terms of outage probabilities. A stochastic distributed transmit-power approach was also investigated in [3–5]. These algorithms were framed with only path loss affecting the channel uncertainty. A distributed autonomous power-control algorithm was introduced in [6], where channel reuse is maximized. Based on a linear analysis of the system, and constraining the eigenvalues, the power approaches an optimal power vector. A generalized framework for uplink power control is provided in [8], where common properties for interference

constraints are identified. An upper limit for the power was imposed for each user in the constrained power-control algorithm of [7]. Active link protection (ALP) schemes were introduced in [11] and [13], where the QoS of active links is maintained above a threshold limit to protect the link quality. An optimum power controller for multicell CDMA wireless networks was designed in [12], where the channel was assumed to be slowly varying without fading.

In [15–20] power control algorithms are designed for systems with radio channel uncertainties caused by mobility of the user terminals. These channel uncertainties include exponential path loss, shadowing, and multipath fading, which are modeled as random variables in the signal-to-interference plus noise ratio (SINR) measurements. Optimization-based approaches that can provide features such as outage guarantees, robustness, and power minimization in the presence of fading but that require knowledge of all channel gains are presented in [15–19]. A distributed power-control scheme was suggested in [20]; however, the fading process is modeled as slowly changing so that the channel gain can be accurately estimated, and practical limitations on the transmission power are not considered.

Multipath fading has the most critical effect on the design of a power-control system because of the time and amplitude scales. Multipath fading is caused by reflections in the environment, which cause multiple time-delayed versions of the transmitted signal to add together at the receiver. The time offsets cause the signals to add with different phases, and thus multipath fading can change significantly over distance scales as short as a fraction of a wavelength. For instance, for a system using the 900 MHz cellular band, the channel coherence time (the time for which the channel is essentially invariant) for a MT traveling at 30 miles/hour is approximately 10 ms.

To allow the power controller to compensate for fast fading in the channel, channel prediction may be used. Linear models, referred to as autoregressive moving average process with exogenous input (ARMAX), were used in [21, 22] for the power-control

process. In [22], a generalized predictive control method was developed to counter loop-delay in closed loop DS-CDMA power control. A linear prediction method is used in [23] to predict a link parameter. A short term fading prediction is done in [24, 25]. Hallen et al. focused on long-range fading prediction [26–28] based on the fact that the amplitude, frequency and phase of each multipath component vary much slower than the actual fading coefficient. The focus of Chapter 2 is to develop a SINR-based power-control algorithm that would reduce the outage probability in the radio link by predicting the power of the channel. The prediction-based power-control process is developed based on the evolution of radio-link parameters from the SINR dynamics and the available feedback SINR measurements.

In Chapter 2, the radio channel characteristics discussed above are analyzed, and the fading power is predicted and used in the control design. For this purpose, a linear minimum mean-square error (LMMSE) predictor is used to obtain a reliable prediction of the fading coefficient at the next instance. In our previous work [29], the predictor used measurements of the fading process. In practice, only the SINR can be measured directly. A LMMSE predictor is developed that uses only SINR measurements and estimates of the Doppler frequency that can be derived from local SINR measurements, inclusive of path loss and shadowing. The motivation behind using the SINR measurements alone is that it is not possible to calculate the fading power from the SINR measurements when the latter is affected by shadowing, path loss, and interference in addition to fast fading. A Lyapunov-based analysis is performed to provide an ultimate bound on the SINR error, the size of which can be reduced by choosing appropriate control gains. In addition, variations in other components of the radio channel such as path loss and log-normal shadowing are also accounted for using this analysis tool. The controller uses local SINR measurements [6], [11] from the current and neighboring cells to maintain the SINRs of MTs in the acceptable communication range, provided channel gains are limited to some practical region of operation. The real channel gains may be arbitrarily low, in which

case no power control algorithm can achieve the desired performance due to limits on the available power. In these cases, the controller may not be able to regulate the SINR into the desired range, and *outage* may occur, where the SINR falls too low for acceptable communication. Simulation is used to assess the performance of the proposed prediction and power-control algorithm. The effects of the choice of prediction window size and quantization of the power-control command are assessed. In addition, the performance is compared with a previously proposed up/down power control algorithm from the literature [30].

In the Medium Access Control (MAC) layer of a wireless network, collisions due to transmission of packets by more than one node to the same receiver results in packet drops at the receiver. Such aberrations occur due to the presence of sensing delays in Carrier Sense Multiple Access (CSMA) networks, and presence of Hidden terminals (HTs) in the network. In addition, queueing constraints of the packets in the Transport Layer of a network causes congestion and delays of packets in the node.

There has been a significant effort to model various forms of CSMA protocols over the past few years [31–33]. Work on MAC layer throughput optimization focuses on manipulating specific parameters of the MAC layer including, for example, window sizes and transmission rates, to maximize / optimize the throughput in the presence of constraints. For example, Carrier Sense Multiple Access (CSMA) Markov chain based throughput modeling and analysis of the MAC algorithms were introduced in [31, 32], while performance and throughput analysis of the conventional Binomial exponential backoff algorithms have been investigated in [34, 35]. In most cases, previous MAC-layer optimization algorithms have focused primarily on parameters and feedback from the MAC layer by excluding collisions during the analysis (cf. [31, 33]). In Chapter 3, we develop a continuous-time Markov model for a system using CSMA that incorporates the effect of collisions and allows optimization of the transmission rates of the network to maximize throughput or meet specified throughput targets. The purpose of this work is

to develop approaches that will be useful in future cross-layer optimization and control algorithms.

Preliminary work on CSMA throughput modeling and analysis was done in [31] based on the assumption that the propagation delay between neighboring nodes is zero. A continuous Markov model was developed that provided the framework and motivation for this work. In [33], a collision-free model is used to quantify and optimize the throughput of the network. The feasibility of the arrival rate vector guarantees the reachability of maximum throughput, which in turn satisfies the constraint that the service rate is greater than or equal to the arrival rate, assuming that the propagation delay is zero. In general communication networks, effects of propagation delay play a crucial role in modeling and analyzing the throughput of the network. Recent efforts attempted various strategies to include delay models in the throughput model. For example, in [36], delay is introduced, and is used to analyze and characterize the achievable rate region for static CSMA schedulers. Collisions, and hence delay is incorporated in [37] in the Markov model, and the mean transmission length of the packets is used as the control variable to maximize the throughput. In this dissertation, a model for propagation delay is proposed and incorporated in the model for throughput. This model allows for the transmission rates to be selected to maximize throughput in an unconstrained optimization problem and to meet feasible throughput goals in a constrained optimization problem. In addition, collisions due to hidden terminals in the network are also modeled and analyzed. Link throughput is optimized by optimizing the waiting times in the network.

Queue length management in dynamic networks such as the Internet has been a longstanding research focus. Several queueing network models have been proposed for such networks to perform congestion control. In [38], a widely used framework was introduced for modeling the Internet where each flow is associated with a utility function and the objective is to maximize the aggregate utility subject to link constraints. Thereafter, in [39] and [40], a review of a class of primal-dual algorithms was performed and design

guidelines were provided for such algorithms that feature dynamic adaptations at both ends of a decentralized end-to-end congestion network. An Exponential Random Early Detection (E-RED) was developed that modifies the standard TCP-Reno and Random Early Detection (RED) algorithms.

The problem of input traffic based modeling of internet-style networks was addressed in [41] with an emphasis on queue length evolution and server rate limitations. Multi-service architectures for the Internet such as IntServ and DiffServ architectures (cf. [42, 43]) have also been an area of recent interest. These architectures characterize the packets based on their loss and delay requirements, and hence prioritize based on the QoS needed. Tipper et. al (cf. [41]) developed differential equation models based on the approximate model of [44] that describe the behavior of the network by time-varying probability distributions and a nonlinear differential model for representing the dynamics of the network in terms of time-varying mean quantities (cf. [41]) for computer networks under nonstationary conditions. Such models are also known as Fluid Flow Models (FFM).

Control efforts in such FFMs focus on providing queue management services. Classical linear analysis techniques were employed in [45] for Asynchronous Transfer Mode (ATM) congestion control problems, and the usage of probabilistic feedback showed better performance in the sense of reducing steady state oscillations. Analytical models were introduced for ATM Routing in [46] and control and optimization algorithms were suggested. A stochastic linear model for flow in networks was studied from a control theoretic perspective in [47]. Subsequently, in [48–50], linear analysis techniques were employed for congestion control problems. Adaptive flow controllers for high resource utilization were developed in [51] and [52]. Nonlinear flow controllers were introduced in [53–55] for ATM based networks using the framework introduced by [41] and [44]. Most of these techniques introduced were heuristic with elaborate simulations to demonstrate the system behavior. An Integrated Dynamic Congestion Controller (IDCC) was developed in [56] based on adaptive nonlinear control techniques, and Lyapunov-based congestion

control development was introduced. An ultimately bounded stability result is obtained by assuming that the derivative of the ensemble average arrival rate is bounded by a finite constant. A sliding mode variable structure congestion controller was utilized in [57] based on the FFM. In [58], a second order sliding mode controller was introduced that claimed that the ensemble average arrival rate for premium service was unknown while using the same in the controller. Recently, a new class of continuous controllers were developed that asymptotically stabilizes a class of nonlinear systems in the presence of bounded sufficiently smooth disturbances (cf. [59, 60]). By using the RISE design approach, a continuous congestion control strategy is developed in Chapter 4 using only the error measurements between the actual and the desired ensemble average queue length for Premium Traffic Service for DiffServ networks. This approach is different from [57] in the sense that the controller is *continuous*, and *global asymptotic regulation* of the ensemble average queue length in the Premium Service buffer is obtained. The inevitable presence of delay in the arrival rates due to propagation and processing is addressed in the control development for Ordinary Services, and *global asymptotic regulation* of the ensemble average queue length in the Ordinary Service buffer is obtained.

CHAPTER 2

POWER CONTROL FOR CELLULAR COMMUNICATIONS WITH TIME-VARYING CHANNEL UNCERTAINTIES

Power control in a code-division multiple access (CDMA) based cellular network is a challenging problem because the communication channels change rapidly because of multipath fading. These rapid fluctuations cause detrimental effects on the control efforts required to regulate the signal-to-interference plus noise ratios (SINRs) to the desired level. Thus, there is a need for power-control algorithms that can adapt to rapid changes in the channel gain caused by multipath fading. Much of the previous work has either neglected the effects of fast fading, assumed that the fading is known, or assumed that all the link gains are known. In this chapter, we model the effects of fast fading and develop practical strategies for robust power control based on SINR measurements in the presence of the fading. We develop a controller for the reverse link of a CDMA cellular system, and use a Lyapunov-based analysis to prove that the SINR error is globally uniformly ultimately bounded. We also utilize a linear prediction filter that utilizes local SINR measurements and estimates of the Doppler frequency that can be derived from local SINR measurements to improve the estimate of the channel fading used in the controller. The power-control algorithm is simulated for a cellular network with multiple cells, and the results indicate that the controller regulates the SINRs of all the mobile terminals (MTs) with low outage probability. In addition, a pulse-code-modulation technique is applied to allow the control command to be quantized for feedback to the transmitter. Simulation results indicate that the outage probabilities of all the MTs are still within the acceptable range if at least 3-bit quantization is employed. Comparisons to a standard algorithm illustrate the improved performance of the predictive controller.

2.1 Network Model and Properties

We consider the reverse link of a cellular system employing CDMA. The SINR $x_i(l) \in \mathbb{R}$ is defined (in dB) for each radio link $i = 1, 2, \dots, n$, as

$$x_i(l) = 10 \log \left(\frac{a g_i(l) P_i(l)}{I_i(l)} \right), \quad (2-1)$$

where $l \in \mathbb{Z}$, the function $\log(\cdot)$ denotes the base 10 logarithm, $g_i(l) \in \mathbb{R}$ is the channel gain in the radio link between MT i and the Base Station (BS), $P_i(l) \in \mathbb{R}$ is the power transmitted by MT i to the BS, $a \in \mathbb{R}$ is the bandwidth spreading factor or the processing gain [61] defined as the ratio of the transmission bandwidth (in Hertz) to the data rate (in bits/second), and $I_i(l) \in \mathbb{R}$ is the interference from the MTs in all the cells, defined as

$$I_i(l) = \sum_{j \neq i} g_j(l) P_j(l) + \eta_i. \quad (2-2)$$

In (2-2), $\eta_i \in \mathbb{R}$ denotes the thermal noise power in link i , which is assumed to be a constant value greater than zero. Since the noise power is bounded and the interference power from each MT is less than its transmit power, $I_i(\cdot)$ is non-zero and bounded.

The channel gain $g_i(l)$ in (2-1) is modeled as [62]

$$g_i(l) = g_{d_0} \left(\frac{d_i(l)}{d_0} \right)^{-\kappa} 10^{0.1\delta_i(l)} |H_i(l)|^2. \quad (2-3)$$

In (2-3), $g_{d_0} \in \mathbb{R}$ is the near-field gain (see [63] for model details). The second factor in (2-3) is the exponential path loss, which depends on the the distance $d_i(l) \in \mathbb{R}$ from MT i to the BS and the path-loss exponent, $\kappa \in \mathbb{R}$, which typically takes values between two and five. Exponential path loss holds in a region outside the near-field region (i.e., the region satisfying $d_f \leq d_0 \leq d_i(l)$, where d_f is the Fraunhofer distance). MTs cannot travel within distance d_0 of the BS and only communicate with the BS if they are within a predetermined radius of coverage, so $d_i(\cdot)$ is non-zero and bounded within a particular operating cell. The factors $10^{0.1\delta_i(l)}$ and $|H_i(l)|^2$ in (2-3) are used to model large-scale

log-normal shadowing (from buildings, terrain, or foliage) and small-scale multipath fading, respectively.

For analytical purposes, the shadowing is generally modeled as log-normal; i.e., $\delta_i(l) \in \mathbb{R}$ is a Gaussian random process. The fading is often modeled as Rayleigh fading, where $H_i(t)$ is usually taken to be a zero-mean, complex-valued, wide-sense stationary Gaussian random process [63], and thus $|H(t)|$ is a Rayleigh random variable for each t . However, both of these processes are unbounded, which means that any non-negative channel gain is possible, and hence any received power level is possible. However, $g_i(l)$ cannot take arbitrarily large values in practice because the received power cannot exceed the transmitted power. Furthermore, a cellular system cannot practically transmit to *overfaded* users who are in very deep fades (i.e., when $g_i(l)$ is close to zero) because doing so would require extremely large power at that user and the other users (because the power transmitted to each user causes interference at the other users) [64]. Hence, the subsequent control-system development is based on the assumption that the shadowing gain $10^{0.1\delta_i(l)}$ and fading gain $|H_i(\cdot)|^2$ are both bounded from above and below. However, the performance is simulated in [section 2.5](#) and [section 2.6](#) for channels that may result in arbitrarily low signal levels, which may result in the power-control algorithm failing to regulate the SINR to the desired region.

Understanding how the SINR changes is beneficial for the development and analysis of the subsequent power-control law. Taking the first difference of (2-1) yields

$$\begin{aligned} \frac{\Delta x_i(l)}{T_s} &= \frac{[10 \log(ag_i(l+1)) - 10 \log(ag_i(l))]}{T_s} \\ &\quad + \frac{u_i(l)}{T_s} - \frac{[10 \log(I_i(l+1)) - 10 \log(I_i(l))]}{T_s}, \end{aligned} \quad (2-4)$$

where T_s is the sampling time of the network, and $u_i(l) \in \mathbb{R}$ denotes an auxiliary control signal defined $\forall i = 1, 2, \dots, n$ as

$$u_i(l) \triangleq 10 [\log(P_i(l+1)) - \log(P_i(l))], \quad (2-5)$$

which is used to determine the power update law. The SINR at the next update interval $x_i(l+1) \in \mathbb{R}$ can then be expressed as

$$x_i(l+1) = \varrho_i [g_i(l+1), I_i(l+1)] - \varrho_i [g_i(l), I_i(l)] + x_i(l) + u_i(l), \quad (2-6)$$

where the functional $\varrho_i \in \mathbb{R}$ is defined $\forall i = 1, 2, \dots, n$ as

$$\varrho_i(y_i, z_i) = 10 \log \left(\frac{ay_i}{z_i} \right). \quad (2-7)$$

2.2 Linear Prediction

The development of a power controller for radio links in a CDMA network is challenging due to rapid, large scale changes in SINR and is exacerbated by a constraint that each link's transmit power is less than some $P_{\max} \in \mathbb{R}$. In this chapter, we attempt to improve performance by estimating the SINR $ag_i(l+1)/I_i(l+1)$ to compensate for the delays in measurement and control. Note that the various channel components that contribute to the SINR, such as fading and shadowing power and path loss are not computable from the received SINR, which motivates our design based on the SINR.

Let $X_i(\cdot) \triangleq g_i(l)/I_i(l)$. We use linear minimum mean-square error (LMMSE) prediction of $X_i(l)$ given n_1 past values, $X_i(l-1), X_i(l-2), \dots, X_i(l-n_1)$. The LMMSE estimator is [65]

$$\hat{X}_i(l) = \sum_{m=l-n_1}^{l-1} \beta_i^{(m)} \{X_i(m) - \mu\} + \mu \quad (2-8)$$

where the coefficients $\beta_i^{(m)}$ depend on the second-order statistics of $X_i(l)$, μ is the mean of the random process $X_i(\cdot)$ for all l . Let $f_i \triangleq \frac{v_i}{\lambda} \cos \theta_i$ be the Doppler frequency of MT i , where v_i is the velocity of motion of the MT, θ_i is the angle between the transmitted signal and the direction of motion of the MT, and λ is the wavelength of the transmitted signal. The Doppler frequency of the MT can be estimated from the SINR measurements (cf. [66]). Let T_p be the prediction observation sampling time, which is selected such that

it is at least the Nyquist rate, i.e., twice the expected maximum of the Doppler frequencies of the MTs [28].

For the subsequent design of the predictor, define $b_i(\cdot) \in \mathbb{R}$ for each radio link i that quantifies the channel without fading, i.e.,

$$b_i(\cdot) = \frac{g_{d_0} \left(\frac{d_i(\cdot)}{d_0} \right)^{-\kappa} 10^{0.1\delta_i(\cdot)}}{I_i(\cdot)}. \quad (2-9)$$

The $\beta_i^{(m)}$'s in (2-8) satisfy the orthogonality condition [65]. Defining $\beta_i \triangleq [\beta_i^{(l-(n_1-1))}, \dots, \beta_i^{(l)}]$ and using the orthogonality condition yields

$$\beta_i^T = \begin{bmatrix} \mathbb{E} [b_i(l)b_i(l-n_1)] \\ \times \mathbb{E} [|H_i(l)|^2 |H_i(l-n_1)|^2] \\ \vdots \\ \mathbb{E} [b_i(l)b_i(l-1)] \\ \times \mathbb{E} [|H_i(l)|^2 |H_i(l-1)|^2] \end{bmatrix}^T Z^{-1}, \quad (2-10)$$

where $Z_{jk} = \mathbb{E} [b_i(l-(n_1-j))b_i(l-(n_1-k)) |H_i(l-(n_1-j))|^2 |H_i(l-(n_1-k))|^2]$ $\forall j, k = 1, 2, \dots, n_1-1$, and we have used the fact that $b_i(\cdot)$ is independent of $|H_i(\cdot)|^2$. Here,

$$\begin{aligned} \mathbb{E} [b_i(l-(n_1-j))b_i(l-(n_1-k))] &= \mathbb{E} \left[\underbrace{\frac{1}{(I_i(l-(n_1-j)))^2}}_{\triangleq R_d} \right] \\ &= \underbrace{\mathbb{E} \left[g_{d_0} \left(\frac{d_i(l-(n_1-j))}{d_0} \right)^{-\kappa} (10^{0.1\delta_i(l-(n_1-j))})^2 \right]}_{\triangleq R_I}, \end{aligned} \quad (2-11)$$

since the numerator in (2-9) is independent of the denominator. R_I results from slow variations in the path loss and shadowing, and hence can be estimated from time averages. Also, the interference during the duration of the prediction sampling can be treated as approximately constant [67], which is a reasonable approximation when the spreading factor is large. Based on these assumptions R_d and R_I are approximated as 1.

The autocovariance function for $|H_i(\cdot)|^2$ is $R_{|H_i|^2}(lT_p) \approx J_0^2(2\pi f_n(lT_p))$ [68], [69], where J_0 is the zeroth-order Bessel function of the first kind, and f_n is the maximum Doppler frequency. Therefore, from (2-10),

$$\beta_i^T = \begin{bmatrix} J_0^2(2\pi f_n(T_p n_1)) \\ J_0^2(2\pi f_n(T_p(n_1 - 1))) \\ \vdots \\ J_0^2(2\pi f_n T_p) \end{bmatrix}^T Z^{-1}, \quad (2-12)$$

where the components of Z are defined $\forall j, k = 1, 2, \dots, n_1$ as

$$Z_{jk} = Z_{kj} = \begin{cases} J_0^2(2\pi f_n(T_p |j - k|)); & j \neq k \\ \sigma_{|H_i|^2}; & j = k \end{cases}, \quad (2-13)$$

$f_n \neq 0$ and $\sigma_{|H_i|^2}$ is the variance of the random process $|H_i(\cdot)|^2$ for all l . The Doppler frequency of each MT is measured periodically and this is used to update the coefficients of the LMMSE estimator. Note that the coefficients of β_i in (2-12) are bounded if the covariance matrix in (2-13) is invertible, which will occur with probability 1 if T_p is less than the Nyquist rate [28]) and the effect of measurement noise is considered. Thus, the linear predictor $\hat{X}_i(\cdot)$ is bounded.

To summarize the algorithm for calculating the channel estimate, an array of previous and current SINR measurements are inputs to the linear predictor rather than the fading power $|H_i(l)|^2$. At every instant, the predictor, based on the available SINR measurements and the autocorrelation model of fading, gives an estimate $\hat{X}_i(l)$ of the quantity $X_i(l)$. In our implementation, the mean of the variable $X_i(l)$ is calculated from 200 initial samples of the SINR measurements and the transmitter power used, and taking the weighted average of $10^{(0.1x_i(m))} / (aP_i(m))$. The constants β_i and Z^{-1} in (2-12) are calculated from the autocovariance function for $|H_i(\cdot)|^2$ (and can be calculated offline and stored for a quantized set of Doppler frequencies). The predicted quantity $\hat{X}_i(l)$ in (2-8) is an input to the controller (refer to section 2.3 and section 2.4 for control development).

Linear prediction of the fading process requires measurement of the $x_i(\cdot)$ at the current and previous instances; the performance of the predictor can be improved by increasing the number of measurements n_1 used to predict the fading process at instance l . Practically, as the number of time samples used in the estimator becomes large, the performance of the predictor does not improve but degrades because the matrix Z becomes ill conditioned.

2.3 Control Development

2.3.1 Control Objective

The network QoS can be quantified by the ability of the SINR to remain within a specified operating range with upper and lower limits, $\gamma_{\min}, \gamma_{\max} \in \mathbb{R}$ for each link defined $\forall i = 1, 2, \dots, n$ as

$$\gamma_{i,\min} \leq x_i(l) \leq \gamma_{i,\max}, \quad (2-14)$$

where $\gamma_{i,\min}$ and $\gamma_{i,\max}$ depend on the quality-of-service requirements of mobile station i . Keeping the SINR above the minimum threshold eliminates signal dropout, whereas remaining below the upper threshold minimizes interference to adjacent cells. The control objective for the following development is to regulate the SINR to a target value $\gamma_i \in \mathbb{R}$ such that $\gamma_{i,\min} \leq \gamma_i \leq \gamma_{i,\max}$, while ensuring that the SINR remains between the specified lower and upper limits for each channel. To quantify this objective, a regulation error $e_i(l) \in \mathbb{R}$ is defined as

$$e_i(l) = x_i(l) - \gamma_i, \quad \forall i = 1, 2, \dots, n. \quad (2-15)$$

2.3.2 Closed-Loop Error System

By taking the first difference of (2-15), using (2-3), (2-6), and (2-7), and properties of the $\log(\cdot)$ function, the open-loop error dynamics for each link can be determined as

$$\Delta e_i(l) = \chi_{gi}(l+1) - \chi_{gi}(l) + u_i(l), \quad (2-16)$$

where the auxiliary function $\chi_{gi}(\cdot) \in \mathbb{R}$ is defined $\forall i = 1, 2, \dots, n$ as

$$\chi_{gi}(\cdot) = x_i(\cdot) - 10 \log(aP_i(\cdot)) \quad (2-17)$$

where $\sqrt{\sum_{i=1}^n \chi_{gi}^2(\cdot)}$ is bounded based on the explanation in [section 2.1](#).

Based on (2-16) and the subsequent stability analysis, the auxiliary power controller $u_i(l)$ is designed as

$$u_i(l) = -(k_p + k_e) e_i(l) - \hat{Y}_i(l+1) + \chi_{gi}(l), \quad (2-18)$$

where $\hat{Y}_i(l+1) \in \mathbb{R}$ is defined $\forall i = 1, 2, \dots, n$ as

$$\hat{Y}_i(l+1) = 10 \log \left\{ \left| \hat{X}_i(l+1) \right| \right\}, \quad (2-19)$$

and

$$\left| \hat{X}_i(\cdot) \right| \neq 0. \quad (2-20)$$

where $\hat{X}_i(\cdot)$ are given in (2-8), and the prediction observation sampling rate is chosen to be at least the Nyquist rate for (2-20) to hold. From (2-5), (2-18), and (2-19), the power update law for each radio channel is obtained $\forall i = 1, 2, \dots, n$ as

$$[P_i(l+1)]_{dB} = -(k_p + k_e) e_i(l) - 10 \log \left\{ a \left| \hat{X}_i(l+1) \right| \right\} + x_i(l). \quad (2-21)$$

2.4 Stability Analysis

Theorem 1: The power update law in (2-21) ensures that all closed loop signals are bounded, and that the SINR regulation error approaches an ultimate bound $\epsilon \in \mathbb{R}$, which can be decreased with increasing k_p in (2-18) up to the maximum power limits and decreasing the sampling intervals up to practical limits, provided k_e in (2-18) is selected as

$$0 < k_e \leq 1, \quad (2-22)$$

and γ_{\min} and γ_{\max} in (2-14) are chosen appropriately.

Proof. Let $V(e, l) : D \times [0, \infty) \rightarrow \mathbb{R}$ be a positive definite function defined as

$$V(e, l) = \sum_{i=1}^n \frac{1}{2} e_i^2(l). \quad (2-23)$$

Taking the first difference of (2-23), by using the fact that $\Delta(ab) = a\Delta b + b\Delta a + \Delta a\Delta b$, and substituting for (2-16) yields

$$\Delta V = \sum_{i=1}^n e_i(l) [\chi_{gi}(l+1) - \chi_{gi}(l) + u_i(l)] + \Delta e_i^2(l), \quad (2-24)$$

where $\Delta e_i(l)$ is the error between the sampling time for radio link i , and $\sum_{i=1}^n \Delta e_i^2(l)$ is bounded by a constant c , the size of which can be controlled by the sampling time. An analysis for this claim can be developed as in [70], though the subsequent simulation is carried out by choosing a high (and feasible) sampling rate. Substituting (2-18) into (2-24) yields

$$\Delta V \leq \sum_{i=1}^n -k_e e_i^2(l) + \sqrt{\sum_{i=1}^n e_i^2(l) (\chi_{gi}(l+1) - \hat{Y}_i(l+1))^2} + \sum_{i=1}^n -k_p e_i^2(l) + c. \quad (2-25)$$

Note that k_p is used to damp out $\sum_{i=1}^n (\chi_{gi}(l+1) - \hat{Y}_i(l+1))^2$ in (2-25) while k_e is the proportional gain used by the controller where $0 < k_e \leq 1$. By completing the squares and using (2-23), the inequality in (2-25) can be further upper bounded as

$$\Delta V \leq -k_e V + \frac{25\varsigma}{k_p} + c \quad (2-26)$$

where $\varsigma = \sum_{i=1}^n (\chi_{gi}(l+1) - \hat{Y}_i(l+1))^2$ is upper bounded by some positive scalar c_2 , i.e., $\varsigma \leq c_2$ based on the development in section 2.1 and section 2.2. Provided the sufficient condition in (2-22) is satisfied, Lemma 13.1 of [71] can be invoked to conclude that

$$V(e, l) \leq (1 - k_e)^l V(e(l_0), l_0) + \left(\frac{1 - (1 - k_e)^l}{k_e} \right) \left[\frac{25\varsigma}{k_p} + c \right]. \quad (2-27)$$

Based on (2-23) and (2-27), an upper bound for the SINR error can be developed as

$$\sum_{i=1}^n e_i^2(l) \leq \sum_{i=1}^n e_i^2(l_0) (1 - k_e)^l + \left(\frac{1 - (1 - k_e)^l}{k_e} \right) \left[\frac{25c_2}{k_p} + c \right]. \quad (2-28)$$

The assumption that $\chi_{gi}(l) \in \mathcal{L}_\infty$, the fact that $\hat{Y}_i(l) \in \mathcal{L}_\infty$ from section 2.2., (2-19), and (2-20), and the fact that $e_i(l) \in \mathcal{L}_\infty$ from (2-28) can be used to conclude that $u_i(l) \in \mathcal{L}_\infty$ from (2-18), and hence $P_i(l+1) \in \mathcal{L}_\infty$ from (2-21). Based on (2-28), as $l \rightarrow \infty$, the norm-squared SINR error is ultimately bounded as $\epsilon \leq ((25c_2)/(k_e k_p)) + (c/k_e)$. The ultimate bound can be decreased by increasing k_p ; however, the magnitude of k_p is practically restricted by the constraint that $0 < P_{\min} \leq P_i(t) \leq P_{\max}$, and the sampling interval T_s . □

Based on the power constraint, the stability of the system is guaranteed if the given SINR thresholds γ_{\min} and γ_{\max} satisfy the following conditions: $\gamma_{\min} \leq \chi_{g_{\min}} + [P_{\max}]_{dB}$, and $\gamma_{\max} \geq \chi_{g_{\max}} + [P_{\min}]_{dB}$, where $\chi_{g_{\min}} \leq |\chi_{gi}(t)| \leq \chi_{g_{\max}}, \forall i$ from (2-17) and the explanation in section 2.1.

The controller is designed based on the stability analysis, that in-turn uses the nonlinear SINR model defined in (2-6). The bounds on the stochastic uncertainties may be high, and hence high control gains might be required to stabilize the system. Given limited available power, the SINR may go outside the thresholds of γ_{\min} and γ_{\max} . To validate the performance and hence address the feasibility of the controller, a metric known as *Outage Probability*, defined as the probability that the SINR $x_i(l)$ goes below γ_{\min} (i.e., $x_i(l) \leq \gamma_{\min}$), is used. Note that if $x_i(l) \geq \gamma_{\max}$, the radio link achieves better performance (lower error rates) for radio i but might increase the interference to other links. Detailed simulations in section 2.5 and section 2.6 evaluate the performance in terms of outage probabilities.

2.5 Simulation Results

A cellular network topology using the proposed power-control algorithm was simulated with one cell of interest and one tier of six adjacent cells in the typical seven-cell

reuse pattern. Ten MTs were simulated in each cell. The Random-Waypoint model is used to simulate the mobility of the MTs, with the initial topology drawn from the steady state (stationary) distribution (cf. [72], [73]). The mobile velocity at each waypoint is randomly chosen from a uniform distribution between 2 km/hr and 48 km/hr. Thus, the probability density function of the velocity is given by [73] $f_i(v) = \frac{C_h}{v} f_{V|h}^0(v)$, where $f_{V|h}^0(v) = \frac{1}{48 \text{ km/hr} - 2 \text{ km/hr}} = \frac{1}{46 \text{ km/hr}}$ and $C_h = 14.47$ is a normalization constant. The subscript h is used to denote the phase of the MT [73]. The velocity for each of the MTs is obtained using the inverse transform method [74] as

$$v = \exp(3.179r + 0.6931), \quad (2-29)$$

where r is uniformly distributed between 0 and 1. The purpose of the simulation section is to detail the performance of the controller, and this is done by including the plot of the worst-case scenario of the radio-link, i.e., when the Doppler frequency is high (refer to [Figure 2-3](#)). The simulations were repeated 10 times (Monte Carlo Simulations) operating 70 MTs (10 MTs in each of the typical seven-cell reuse pattern) in each simulation so that the data collected for the subsequent analysis is sufficient. Also, each simulation was carried out with fixed control gains k_p and k_e . The *average* value of the outage probabilities of the MTs operating in each of the four maximum Doppler frequency ranges are tabulated (refer to [Table 2-1](#)) along with the feasible window size for various ranges of the Doppler frequencies.

Path loss, with free space propagation effects and log-normal shadowing, is modeled [63] as shown in (2-3). The angle θ is measured periodically, and the Doppler frequency is obtained from (2-29), which is used to generate the Rayleigh fading and update the coefficients of the LMMSE predictor. The channel sampling time (T_s) and prediction observation sampling time (T_p) are both set to 1.7 ms, based on performing a continuous time SINR error analysis [70]. The target SINR, γ was set to 8 dB, with a desired operating range between 6 and 10 dB, which is defined in [subsection 2.3.1](#). Thermal noise,

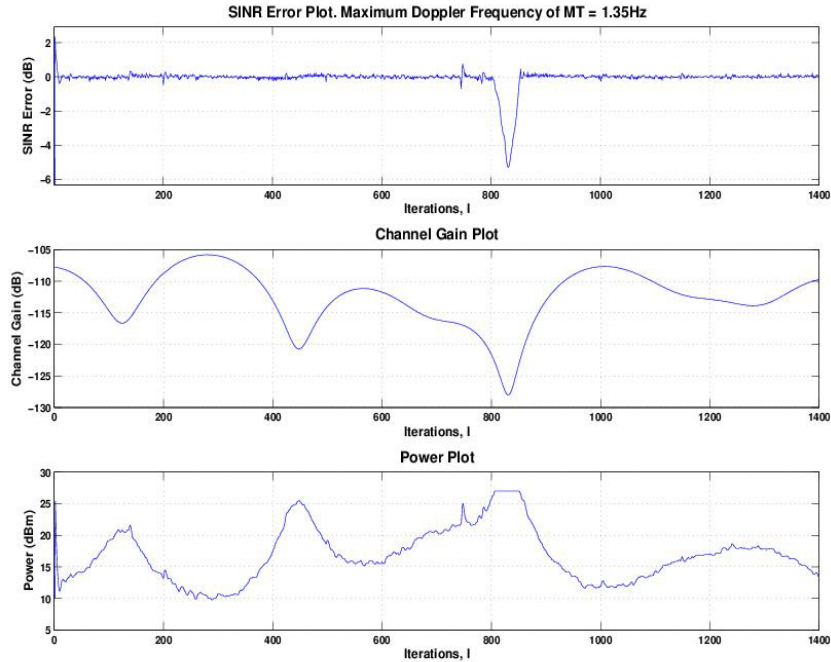


Figure 2-1. Error, channel gain, and power plot of a MT with maximum Doppler frequency 1.35 Hz.

η , was set to -83 dBm. The initial power level for all MTs was chosen as 10 dBm. Also, the prediction window size is updated online to avoid an ill-conditioned matrix Z . Starting at a specified maximum prediction window size, the size of the window is consecutively reduced by 1 until $\det Z \geq 10^{-5}$.

The results in Figs. 2-1-2-4 are obtained with $k_p = 0.65$, $k_e = 1.3 \times 10^{-4}$, and the spreading factor a is chosen as 512, which is the maximum for Wideband CDMA systems. Note that the same values of the control gains and spreading factor are also used in the subsequent simulations. The control gains were tuned using simulations with a different set of random seeds than those used in the performance evaluation. The output of the linear predictor is limited to $\hat{X}_{\max} = 47$ dB for the reasons explained in section 2.2.

Figure 2-1 shows the SINR error, channel gain and power plots of a MT that has a maximum Doppler frequency of 1.35 Hz. Note that the Doppler frequencies in simulations are generated from the aforementioned topology model. A Doppler frequency

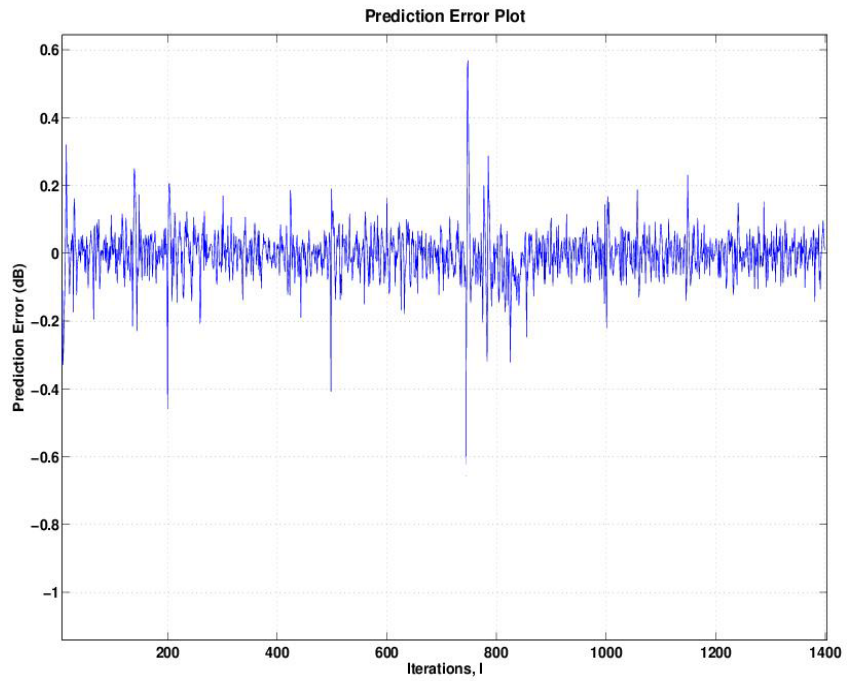


Figure 2-2. Prediction error of the MT with maximum Doppler frequency 1.35 Hz.

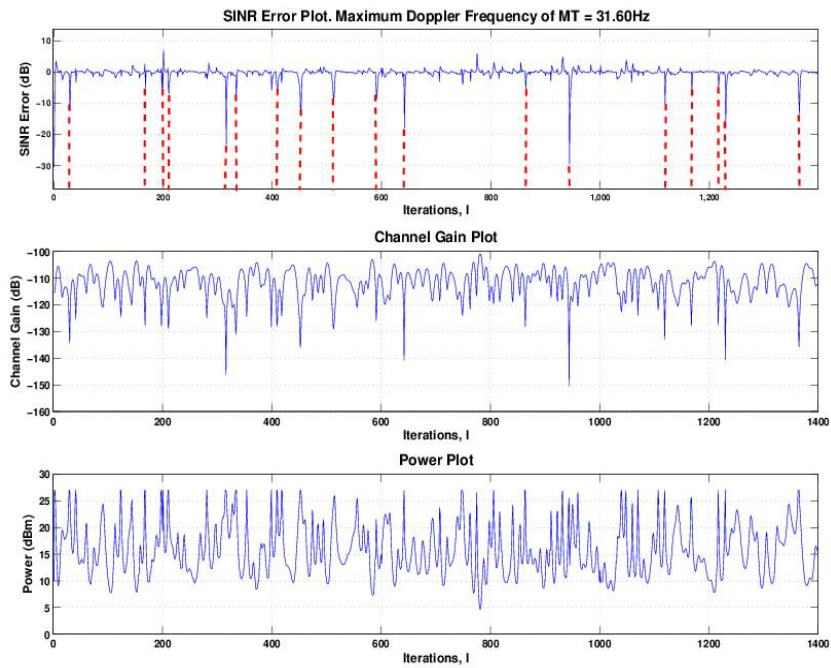


Figure 2-3. Error, channel gain, and power plot of a MT with maximum Doppler frequency 31.60 Hz.

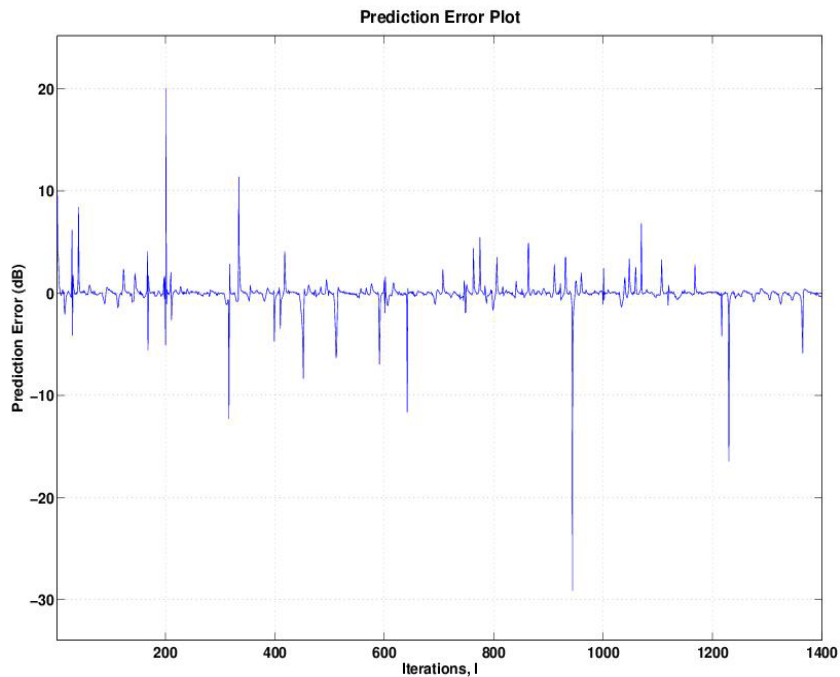


Figure 2-4. Prediction error of the MT with maximum Doppler frequency 31.60Hz.

of 1.35 Hz represents a MT with low mobility. The prediction error for this MT is shown in Figure 2-2. Figure 2-1 indicates that the power controller regulates the SINR of the MT within the desired range ($\gamma_{\min} \leq x_i(\cdot) \leq \gamma_{\max}$) with low outage probability. Figure 2-3 shows the SINR error, channel gain and power plots of a MT operating with a maximum Doppler frequency of 31.60 Hz. A Doppler frequency of 31.60 Hz represents a MT with high mobility¹. The dotted lines note the regions of deep fades, which result in large prediction errors, as shown in Figure 2-4. The inaccuracy of the linear predictor and the limits on maximum transmit power (and, correspondingly, control effort) in the deep faded zones cause outage at the MT at those times. The SINR of this radio link operating with

¹ MTs with higher velocities can rely on time diversity, rather than fading, to operate in a fading channel.

Table 2-1. Comparison against various prediction window sizes.

Max. Doppler frequency range (Hz)	Best window size such that $\det Z \geq \zeta$	Average % of samples such that $x_i \leq \gamma_{\min}$			
		Max. Pred. window size of 1	Max. Pred. window size of 2	Max. Pred. window size of 3	Max. Pred. window size of 4
0 – 10	2	10.62	5.19	–	–
10 – 20	2, 3	15.62	4.01	6.91	–
20 – 30	3	19.94	13.42	7.29	–
30 – 40	3, 4	22.98	9.88	7.00	5.07

a maximum Doppler frequency of 31.60 Hz is in the acceptable communication range at all other times, and the required power is in the implementable range.

Simulations were carried out for prediction-based power-control algorithms with different prediction window sizes based on the same topology model with ten MTs in a cell to compare the results. Table 2-1 shows the average % outages for different ranges of the maximum doppler frequency (cf. [15, 75]) of the MTs when the simulation is carried out using different prediction window sizes. The average % outages for the MTs were computed by running 5-10 simulations and classifying the MTs based on their maximum doppler frequencies (column 1 in Table 2-1). The best window size is the maximum value of the window size so that the matrix Z is not ill-conditioned (i.e., $\det Z \geq \zeta$), and the corresponding average % outage is entered in bold. The maximum doppler frequency is measured frequently (cf. [66] and the references therein), i.e., $400T_s$ in this simulation, and the measured values are used to calculate the linear coefficients β_i^m , $\forall m = 1, 2, \dots, n_1 - 1$. It can be inferred that these bolded values fall within the threshold level for voice communications. For voice communications, the typical outage target is 10% [76].

The results in Table 2-2 show the performance of the predictive control algorithm for different numbers of users per cell. Outage probabilities less than 10% can be achieved for 10, 20, or 40 users per cell. However, the control gain k_p must be increased as the number

Table 2-2. Percentage of sample times experiencing outage for different number of users in the cell of interest. The control gain k_p is tuned for the system based on the number of users, and $k_e = 1.3 \times 10^{-4}$. The prediction window sizes are selected based on the condition $\det Z \geq \zeta$ (refer to Table 2-1 for the best window size selection).

Doppler freq. range (Hz)	Average % of samples where $x_i \leq \gamma_{\min}$		
	10 users	20 users	40 users
0 – 10	1.3	2.2	2.6
10 – 20	2.1	4.1	5.0
20 – 30	5.1	6.1	6.7
30 – 40	5.5	8.4	9.5
Best k_p	0.65	0.7	1
Avg. Transmit Power	–16.47 dBm	–15.51 dBm	–14.75 dBm

of users to achieve this outage probability, and this results in an increase in the average transmitted power per user.

2.6 Power-Control Mechanism

In practice, the number of bits that can be sent for power updates to the mobile terminal is limited. Thus, this section considers the design of a power-control mechanism that selects from a finite set of power adjustments. Various results in the literature focus on developing quantized power-control algorithms [14, 21, 77]. A power-control algorithm with a fixed step size was introduced in [14]. Due to the time-varying nature of the radio channel, the performance of this mechanism is limited. A pulse-code-modulation realization was developed in [77] to reduce the outage probability by varying the range of the power updates. In this section, a power-update mechanism based on the pulse-code-modulation realization is used to update the transmitter power at the mobile terminal, and the outage probabilities of the radio links are compared with the outage probabilities without quantization obtained in section 2.5.

The realization of the power-control command is based on the error signal generated at the BS, as shown in Figure 2-5. The quantization of the error signal is done by analyzing the probability density function (Figure 2-6) of the worst case unquantized

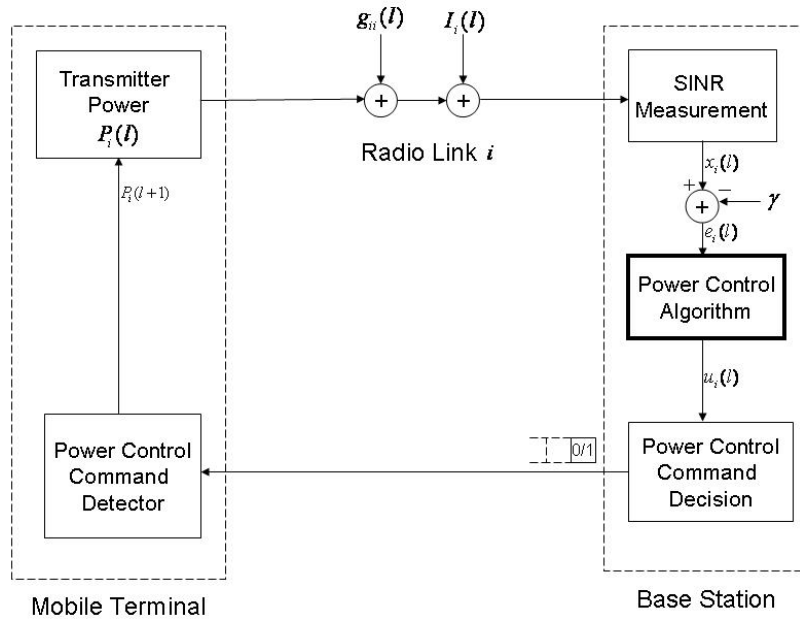


Figure 2-5. Uplink power-control mechanism.

error signals (cf. [section 2.5](#)), i.e., the radio links operating at the high Doppler frequency. Note that the probability density function of the error signal $e(l)$ is represented as $f_E(e)$.

We assume that a power control command is only issued if the error signal is large. The presence of a power control command is usually signaled by a separate control bit (as in IS-95/cdma2000). Thus, for k -bit quantization, $2^k + 1$ levels can be used, where one level maps to a zero command. The error is then quantized by partitioning the empirical density of the error signals that operate at high maximum Doppler frequencies that are obtained from a separate simulation of the unquantized system (to avoid over-training), shown in [Figure 2-6](#), into bins of equal probability. The quantized value of the corresponding control is then defined as the median given that the signal lies in that bin, as that is found to offer better performance than other measures, such as the conditional mean. The quantization scheme depends on the number of bits used for

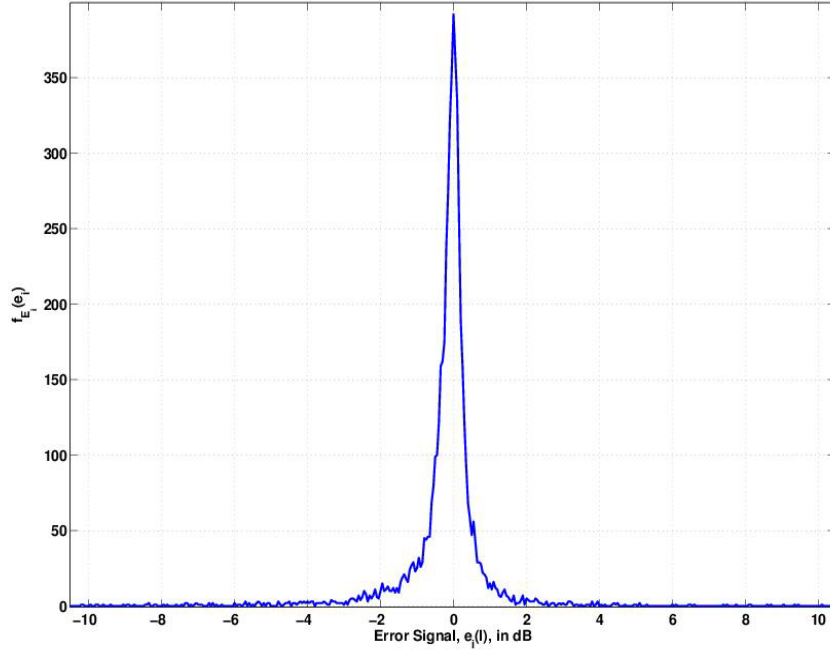


Figure 2-6. Probability density function of the SINR errors of all the MTs operating at high (> 25 Hz) maximum Doppler frequencies

quantization. For 3-bit quantization, the quantized error signal (in dB) is given by

$$u_{pcm_i}(l) = \begin{cases} 3.18 & \text{if } u_i(l) \in (2.08, \infty) \\ 1.47 & \text{if } u_i(l) \in (1.10, 2.08] \\ 0.77 & \text{if } u_i(l) \in (0.44, 1.10] \\ 0.17 & \text{if } u_i(l) \in (-0.07, 0.44] \\ 0 & \text{if } e_i(l) \in (-0.035, 0.035) \\ -0.31 & \text{if } u_i(l) \in (-0.56, -0.07] \\ -0.81 & \text{if } u_i(l) \in (-1.09, -0.56] \\ -1.47 & \text{if } u_i(l) \in (-1.98, -1.09] \\ -3.00 & \text{if } u_i(l) \in (-\infty, -1.98] \end{cases} . \quad (2-30)$$

For 2-bit quantization, the quantized error signal (in dB) is given by

$$u_{pcm_i}(l) = \begin{cases} 2.08 & \text{if } u_i(l) \in (1.10, \infty) \\ 0.44 & \text{if } u_i(l) \in (-0.07, 1.10] \\ 0 & \text{if } e_i(l) \in (-0.035, 0.035) \\ -0.56 & \text{if } u_i(l) \in (-1.09, -0.07] \\ -1.98 & \text{if } u_i(l) \in (-\infty, -1.09] \end{cases} . \quad (2-31)$$

The thresholds on the error when no power control command is issued is tuned (to $\pm 0.035dB$, in this case) based on repeated simulation of the unquantized system, quantizing the control signal, simulation of the quantized system, and performance analysis in terms of outage probability.

Monte Carlo Simulations were carried out on the network topology as described in [section 2.5](#), using the 2-bit ($2^2 = 4$ combinations) and 3-bit ($2^3 = 8$ combinations) quantized error signals to determine the n -bit power control command decision that is provided to the MT. Results were obtained by first simulating using the unquantized power controller (i.e., power controller with infinite feedback bandwidth). Another simulation is carried out by seeding the preceding simulation using the same random seeds, but now using a 2-bit feedback. Similarly, results are obtained for a 3-bit feedback. Then, 10 new simulations are executed using the unquantized controller, and the above mentioned process is repeated for 2-bit and 3-bit feedback. Data is collected, stored and tabulated in [Table 2-3](#). [Table 2-3](#) shows the *average* outage probability of the various schemes (unquantized, 2-bit, and 3-bit power control command) obtained from such repeated simulations to compare and choose the best (in terms of reducing the outage probability) possible quantization scheme based on the bandwidth constraints. From [Table 2-3](#), a 3-bit power control command signal provides performance that falls in the acceptable region for voice communication, and hence this scheme can be used in conjunction with the controller to deliver the desired QoS for each radio link. Note that the control gains k_p and k_e are fixed throughout the course of the simulations.

Table 2-3. Percentage of sample times experiencing outage for unquantized, 2-bit and 3-bit power-control commands.

Doppler freq. range(Hz)	Average % of samples where $x_i \leq \gamma_{\min}$		
	Unquantized control command	3-bit command	2-bit command
0 – 10	1.3	1.4	1.5
10 – 20	2.1	2.7	3.8
20 – 30	5.1	7.3	11.5
30 – 40	5.5	9.8	13.6

We compared the performance of our control algorithm with the up/down power control algorithm described and analyzed in [30]. The up/down power control algorithm uses 1-bit feedback to determine whether to adjust the power up or down by a fixed 0.5 dB. We compare the performance of the up/down power controller to the power control algorithm developed in this chapter both with and without channel prediction. The results are illustrated in Figure 2-7. The results show that the use of 3-bit feedback with our control algorithm provides substantial gains over the 1-bit up/down control algorithm for all mobile velocities. For Doppler frequencies over 10 Hz, the use of channel prediction provides a significant additional performance gain, especially at high Doppler frequencies. For instance for mobile radios with Doppler frequencies between 30 Hz and 40 Hz, the up/down power controller has outage probability over 0.22. Using the power control algorithm developed in this chapter, but without channel prediction, lowers the outage probability to less than 0.19. The addition of channel prediction further lowers the outage probability to less than 0.1, thereby satisfying the typical target outage probability for mobile voice communications. Thus, the benefits of using channel prediction and multi-bit feedback are demonstrated.

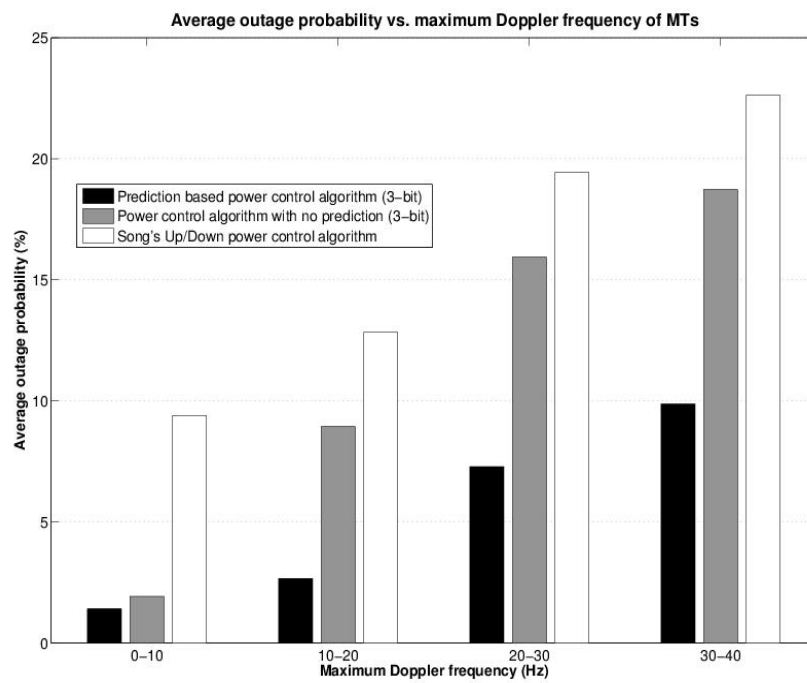


Figure 2-7. Comparison against Song's power control algorithm.

CHAPTER 3 THROUGHPUT MAXIMIZATION IN CSMA NETWORKS

3.1 Throughput Maximization in CSMA Networks with Collisions

In MAC layer of a wireless network that uses CSMA, the performance is limited by collisions that occur because of carrier sensing delays associated with propagation and the sensing electronics. In this chapter, a continuous-time Markov model is used to analyze and optimize the performance of a system using CSMA with collisions caused by sensing delays. The throughput of the network is quantified using the stationary distribution of the Markov model. An online algorithm is developed for the unconstrained throughput maximization problem. Further, a constrained problem is formulated and solved using a numerical algorithm. Simulations are provided to analyze and validate the solution to the unconstrained and constrained optimization problems.

3.1.1 Network Model

Consider an infrastructure network, such as a wireless local area network (WLAN), consisting of an access point and n mobile stations. There are n links connecting the stations to the AP, as shown in Fig. 3-1. All of the nodes in the network are assumed to sense the transmissions of all of the other nodes, provided that the transmissions do not begin within a fixed sensing delay, δT_s . If two or more nodes initiate packet transmission within δT_s , there will be a collision, and all of the packets involved in the transmission are assumed to be lost. In a typical CSMA network, the transmitter of node k backs off for a random period before it sends a packet to its destination node, if the channel is idle. If the channel is busy, the transmitter freezes its backoff counter until the channel is idle again. It is assumed that the backoff time, or the waiting time of each link k is exponentially distributed with mean $1/R_k$. The objective in this chapter is to determine the optimal values of the mean transmission rates R_k , $k = 1, 2, \dots, n$, so that the throughput in the network is either maximized (if all of the nodes are assumed to have the same traffic requirements) or so that the throughput requirements of the nodes are met (if feasible).

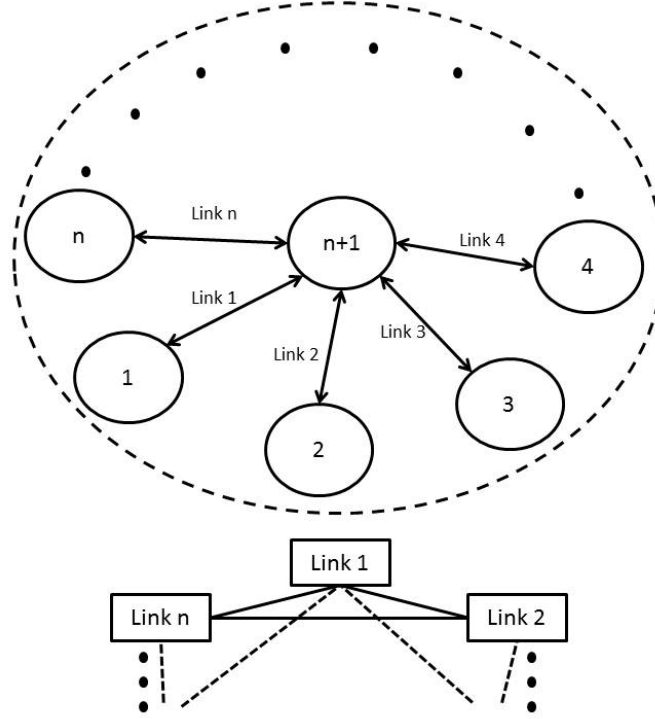


Figure 3-1. A n -link network scenario and conflict graph.

For this purpose, a Markovian model is used, and its states, defined as $x^i \in \{0, 1\}^n$, represents the status of the network where 1 represents an active link, and 0 represents an idle link. For example, if the k th link in state i is active, then $x_k^i = 1$.

Two sets of indices are defined below for the collision-free transmission states, \mathcal{A} , and the collision states, \mathcal{C} :

$$\mathcal{A} = \left\{ i \mid \sum_{k=1}^n x_k^i = 1 \right\}$$

$$\mathcal{C} = \left\{ i \mid \sum_{k=1}^n x_k^i > 1 \right\}$$

where $x_k^i = \begin{cases} 1 & \text{if link } k \text{ in state } i \text{ is active,} \\ 0 & \text{otherwise.} \end{cases}$

Previous work in this field assumed that the propagation delay between neighboring nodes is zero (cf. [31, 33]), and hence, the motivation behind this chapter is to maximize the throughput in the network in the presence of sensing delays, and consequently

collisions. Although collisions due to hidden terminals are possible, this chapter focuses on collisions due to sensing delay. Nevertheless, the formulations in this chapter can be extended to hidden terminals as well using the formulations of the rate of transitions in [31]. The following section explains the continuous CSMA Markov chain in detail.

3.1.2 CSMA Markov Chain

Formulations of Markov models for capturing the MAC layer dynamics in CSMA networks were developed in [31, 32]. The stationary distribution of the states and the balance equations were developed and used to quantify the throughput. Recently, a continuous time CSMA Markov model without collisions was used in [33] to develop an adaptive CSMA to maximize throughput. Collisions were introduced in [37] in the Markov model, and the mean transmission length of the packets are used as the control variable to maximize the throughput. Since most applications experience random length of packets, the transmission rates (packets/unit time), R_k , $k = 1, 2, \dots, n$, of the links are used as a practical measure in this chapter.

The model for the waiting times is based on the CSMA random access protocol. The probability density function of the waiting time T_k is given by

$$f_{T_k}(t_k) = \begin{cases} R_k \exp(-R_k t_k) & \text{for } t_k \geq 0, \\ 0 & \text{for } t_k < 0. \end{cases} \quad (3-1)$$

Due to the sensing delay experienced by the nodes in the network, the probability that link k becomes active within a time duration of δT_s from the instant link l becomes active is

$$p_{c_k} \triangleq 1 - \exp(-R_k \delta T_s) \quad (3-2)$$

by the memoryless property of the exponential random variable. Thus, the rate of transition G_i to one of the non-collision states in the Markov chain in Fig. 3-2 is defined as

$$G_i = \sum_{k=1}^N \left(x_k^i R_k \prod_{l \neq k} (1 - p_{c_l})^{(1-x_l^i)} \right) \quad \forall i \in \mathcal{A}. \quad (3-3)$$

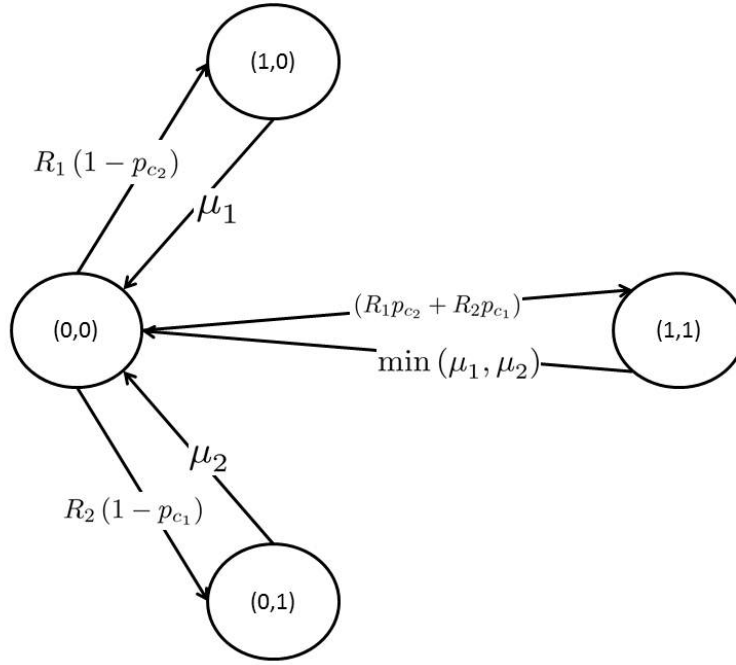


Figure 3-2. CSMA Markov chain for a 2-link scenario with collision states.

The rate of transition G_i to one of the collision states is given by

$$G_i = \sum_{k=1}^N \left(x_k^i R_k \prod_{l \neq k} (p_{cl})^{x_l^i} (1 - p_{cl})^{(1-x_l^i)} \right) \quad \forall i \in \mathcal{C}. \quad (3-4)$$

The state (1, 1) in Fig. 3-2 represent the collision state, which occurs when a link tries to transmit within a time span of δT_s from the instant another link starts transmitting.

The primary objective of modeling the network as a continuous CSMA Markov chain is to maximize the probability of being in the collision-free transmission states. For this purpose, the stationary distribution of the continuous time Markov chain is defined as

$$p(x^i) \triangleq \frac{\exp(r_i)}{\sum_j \exp(r_j)}, \quad (3-5)$$

where

$$r_i \triangleq \begin{cases} \ln \left\{ \frac{\sum_{k=1}^n \left(x_k^i R_k \prod_{l \neq k} (1-p_{c_l})^{(1-x_l^i)} \right)}{\sum_{k=1}^n x_k^i \mu_k} \right\} & \text{for } i \in \mathcal{A}, \\ \frac{\sum_{k=1}^n \left(x_k^i R_k \prod_{l \neq k} (p_{c_l})^{x_l^i} (1-p_{c_l})^{(1-x_l^i)} \right)}{\min_{m: x_m^i \neq 0} (\mu_m)} & \text{for } i \in \mathcal{C}, \\ 1 & \text{otherwise.} \end{cases} \quad (3-6)$$

where $1/\mu_i$ is the mean transmission length of the packets if the network is in one of the states in set \mathcal{A} . The set $\mathcal{A} \triangleq \mathcal{C}^c \setminus (0,0)^T$ represent the set of all collision-free transmission state indices, where the elements in the set \mathcal{C} represent the collision state indices, and the elements in the set \mathcal{C}^c represent the non-collision state indices. In (3-6), the definitions for the rate of transitions in (3-3) and (3-4) are used, and (3-5) satisfies the detailed balance equation (cf. [78]).

3.1.3 Throughput Maximization

To quantify the throughput, a log-likelihood function is defined as the summation over all the collision-free transmission states as

$$F(R) \triangleq \sum_{i \in \mathcal{A}} \ln(p(x^i)). \quad (3-7)$$

By using the definition for $p(x^i)$ in (3-5), the log-likelihood function can be rewritten as

$$\begin{aligned} F(R) &= \sum_{k=1}^n \ln \left(\frac{R_k}{\mu_k} \right) - (n-1) \sum_{k=1}^n R_k \delta T_s - n \ln \left[\sum_{k=1}^n \frac{R_k}{\mu_k} \prod_{l \neq k} \exp(-R_l \delta T_s) \right. \\ &\quad \left. + \sum_{i \in \mathcal{C}} \exp \left(\frac{1}{\min_{m: x_m^i \neq 0} (\mu_m)} \sum_{k=1}^n \left(x_k^i R_k \prod_{l \neq k} (p_{c_l})^{x_l^i} (1-p_{c_l})^{(1-x_l^i)} \right) \right) \right. \\ &\quad \left. + \exp(1) \right]. \end{aligned} \quad (3-8)$$

For example, the log-likelihood function in (3-7) for a 2-link scenario can be expressed as

$$\begin{aligned}
F(R_1, R_2) &= \ln\left(\frac{R_1}{\mu_1}\right) - R_2\delta T_s + \ln\left(\frac{R_2}{\mu_2}\right) - R_1\delta T_s \\
&\quad - 2\ln\left[\exp\left(\ln\left(\frac{R_1 \exp(-R_2\delta T_s)}{\mu_1}\right)\right)\right] \\
&\quad + \exp\left(\ln\left(\frac{R_2 \exp(-R_1\delta T_s)}{\mu_2}\right)\right) + \exp\left(\frac{1}{\min(\mu_1, \mu_2)}\right. \\
&\quad \left.(R_1(1 - \exp(-R_2\delta T_s)) + R_2(1 - \exp(-R_1\delta T_s))) + \exp(1)\right].
\end{aligned}$$

The function $F(R)$ in (3-8) is concave, since natural logarithms and summation of concave functions is a concave function (cf. [79]). In addition, $F(R) \leq 0$, since $\ln(p(x^i)) \leq 0$ from the definition of $p(x^i)$ in (3-5). The optimization problem is defined as

$$\max_R (F(R)). \quad (3-9)$$

Taking the partial derivative with respect to R_k in (3-8) yields

$$\begin{aligned}
\frac{\partial F(R)}{\partial R_k} &= \frac{1}{R_k} - (n-1)\delta T_s - \frac{n}{D} \left\{ \frac{1}{\mu_k} \prod_{l \neq k} \exp(-R_l \delta T_s) \right. \\
&\quad - \left(\sum_{m: m \neq k} \frac{R_m}{\mu_m} \prod_{l \neq m, k} \exp(-R_l \delta T_s) \right) \delta T_s \exp(-R_k \delta T_s) \\
&\quad + \sum_{x^i \in \mathcal{C}} \left[\exp\left(\frac{1}{\min_{m: x_m^i \neq 0} (\mu_m)} \sum_{k=1}^N x_k^i R_k \prod_{l \neq k} (p_{c_l})^{x_l^i} (1 - p_{c_l})^{(1-x_l^i)}\right) \right. \\
&\quad \left(\frac{1}{\min_{m: x_m^i \neq 0} (\mu_m)} \left(x_k^i \prod_{l \neq k} (p_{c_l})^{x_l^i} (1 - p_{c_l})^{(1-x_l^i)} \right) \right. \\
&\quad \left. \left. + \left(\sum_{m: m \neq k} x_m^i R_m \prod_{l \neq m, k} (p_{c_l})^{x_l^i} (1 - p_{c_l})^{(1-x_l^i)} \right) \right) \right. \\
&\quad \left. \left. \frac{\partial}{\partial R_k} \left((p_{c_k})^{x_k^i} (1 - p_{c_k})^{(1-x_k^i)} \right) \right) \right] \left. \right\}, \quad (3-10)
\end{aligned}$$

$k = 1, 2, \dots, n - 1$, where

$$D \triangleq \sum_{k=1}^n \exp \left(\ln \left(\frac{R_k \prod_{l \neq k} \exp(-R_l \delta T_s)}{\mu_k} \right) \right) + \sum_{i \in \mathcal{C}} \exp \frac{\sum_{k=1}^N \left(x_k^i R_k \prod_{l \neq k} (p_{cl})^{x_l^i} (1 - p_{cl})^{(1-x_l^i)} \right)}{\min_{m: x_m^i \neq 0} (\mu_m)} + \exp(1). \quad (3-11)$$

An online gradient-based algorithm is used to solve the problem in (3-9). The gradient law is defined as

$$\ln R_k(t + T) = \ln R_k(t) + K \frac{\partial F(R)}{\partial R_k}, \quad (3-12)$$

$k = 1, 2, \dots, n - 1$, where $K \in \mathbb{R}$ is the step size, T is the time interval between updates, and $\partial F(R)/\partial R_k$ is defined in (3-10). The calculation of $\partial F(R)/\partial R_k$ at the transmitter of link k is determined as follows. The transmitting node of link k calculates the steady-state probabilities of the states $p(x^i)$, $\forall i \in \mathcal{A}$ every T unit time. The transmitting node of link k calculates the steady-state probabilities of the collision-free transmission states alone, since these are sufficient to estimate the mean transmission rates R_m , $m \neq k$ using (3-5). For a n -link case, the transmitter of link k needs to solve the following set of independent nonlinear equations (after manipulations of (3-5)),

$$R_l \exp(-R_l \delta T_s) = \left(\frac{\mathbb{P}(\text{Only link } l \text{ is active})}{\exp(-R_k \delta T_s)} \right) \left(\frac{R_k}{\mathbb{P}(\text{Only link } k \text{ is active})} \right), \quad (3-13)$$

$\forall l \neq k$. Note that link k can use its current value of the mean transmission rate R_k to solve (3-13). The value of T can be chosen sufficiently large so that $p(x^i)$, $\forall i \in \mathcal{A}$ can be measured accurately. Further, large T affects identification of the collision-free transmission states by the transmitter of link k using the Carrier Sense (CS) protocol. The maximum sensing delay δT_s and the mean transmission lengths $1/\mu_k$, $k = 1, 2, \dots, n - 1$ are assumed to be known at all the transmitting nodes. Hence, the algorithm is *distributed*.

In addition to maximizing the log-likelihood function, certain constraints must be satisfied. The service rate $S(R)$ at each transmitter of a link needs to be equal to the arrival rate λ , and the chosen mean transmission rates R_k , $k = 1, 2, \dots, n$, need to be non-negative. Thus, the optimization problem can be formulated as

$$\max_R (F(R))$$

subject to

$$\ln \lambda - \ln S(R) = 0, \quad (3-14)$$

and

$$R \geq 0, \quad (3-15)$$

where $R \in \mathbb{R}^n$, $S(R) \in \mathbb{R}^{n-1}$, and $\lambda \in \mathbb{R}^{n-1}$. The service rate for a link is the rate at which a packet is transmitted, and is quantified as

$$S_k(R) \triangleq \frac{\exp \left(\ln \left(\frac{R_k \prod_{l \neq k} \exp(-R_l \delta T_s)}{\mu_k} \right) \right)}{D},$$

$k = 1, 2, \dots, n - 1$, and D is defined in (3-11). Note that $\ln \lambda_k - \ln S_k(R) = 0$, $\lambda_k > 0$ is concave for all k . The optimization problem defined above is a concave constrained nonlinear programming problem, and obtaining an analytical solution is difficult. There are numerical techniques adopted in the literature which have investigated such problems in detail [79–82]. In this work, a suitable numerical optimization algorithm is employed to solve the optimization problem defined in (3-9), (3-14), and (3-15).

The following section analyzes the numerical results obtained by solving the unconstrained problem of (3-9), and compares the mean transmission rates obtained online from the distributed algorithm of (3-12) with the optimal values. Further, numerical analysis of the constrained problem defined in (3-9), (3-14), and (3-15) is performed.

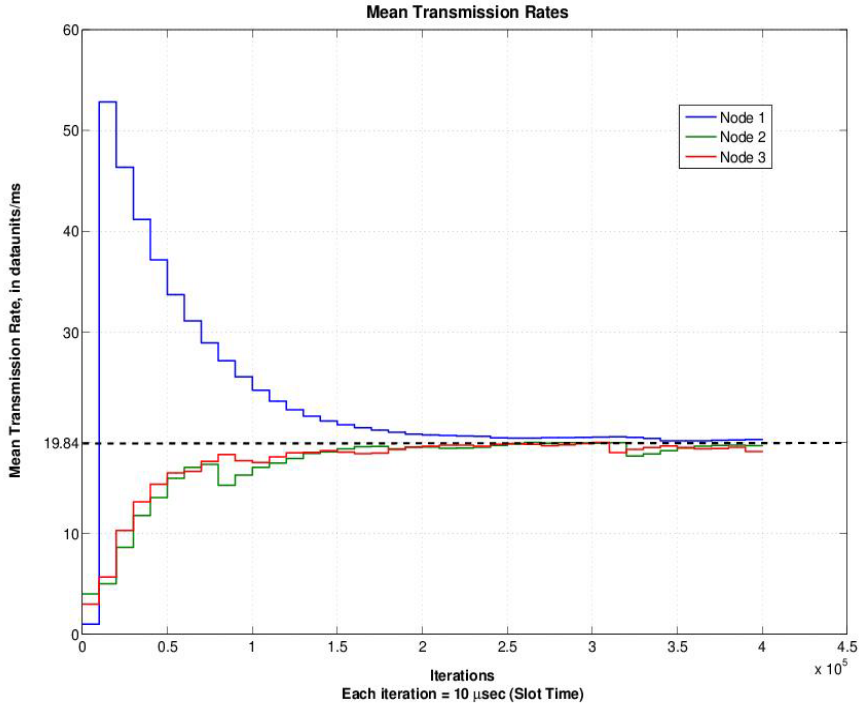


Figure 3-3. Mean transmission rates of nodes 1, 2, and 3 transmitting to the same node 4. All nodes are in the sensing region. The online algorithm of (3-9) is used with $T = 100$ ms, $K = 5$, and $\delta T_s = 0.001$ ms.

3.1.4 Simulation Results

A CSMA platform is developed using MATLAB that uses the standard carrier sense channel access protocol. A slot time of $10 \mu s$ is used, and the mean transmission lengths of the packets, $1/\mu_k$, $k = 1, 2, \dots, n$, are set to 1 ms. An update time of $T = 100$ ms and a step size of $K = 5$ are used. The distributed algorithm in (3-12) is used to generate the rate updates for each transmitting node $k = 1, 2, \dots, n - 1$. The transmitter of link k calculates the steady-state distribution of the states $p(x^i)$, $\forall i \in \mathcal{A}$ every T unit time, and estimates the mean transmission rates of the other transmitting nodes R_m , $m \neq k$ using (3-13) to calculate (3-10). A nonlinear equation solver (MATLAB built-in function `fzero`) can be used to solve (3-13). The mean transmission rate updates can thus be calculated from (3-12). For a 3-link network with sensing delay of 0.001 ms, the mean transmission rates convergence is shown in Fig. 3-3.

The optimal value for the mean transmission rates for a 3-link network is calculated offline for the unconstrained problem of (3-9) for comparison purposes. The MATLAB built-in function `fminunc` is used for this purpose, and the optimal value for the mean transmission rates were obtained as

$$\begin{aligned} R_{1_{\text{opt}}} &= R_{2_{\text{opt}}} = R_{3_{\text{opt}}} \\ &= 19.84 \text{ dataunits/ms.} \end{aligned} \tag{3-16}$$

Fig. 3-3 indicates that mean transmission rates obtained from the online distributed algorithm of (3-12) converge to the optimal values, defined in (3-16).

The online algorithm (3-12) does not take into account the rate constraint defined in (3-15). The constrained concave nonlinear programming problem defined in (3-9), (3-14), and (3-15) is solved by optimizing the mean transmission rates R_k , $k = 1, 2, \dots, n$, of the transmitting nodes in the network of Fig. 3-1 by a suitable numerical optimization algorithm. A MATLAB built-in function `fmincon` is used to solve the optimization problem by configuring it to use the interior point algorithm (cf. [83, 84]).

Once the mean transmission rates are optimized, they are fixed in a CSMA platform (developed in MATLAB) that uses the carrier sense channel access protocol. The function `fmincon` solves the optimization problem only for a set of feasible arrival rates. A slot time of $10 \mu\text{s}$ is used, and the mean transmission lengths of the packets, $1/\mu_k$, $k = 1, 2, \dots, n$, are set to 1 ms. Further, a stable (and feasible) set of arrival rates, in the sense that the queue lengths at the transmitting nodes are stable, are chosen before simulation.

A 2-link collision network is simulated using the platform explained above. The optimal values of the mean transmission rates, R_1 and R_2 , are obtained and tabulated as shown in Table 3-1 for different values of the sensing delay δT_s . Note that the capacity of the channel is normalized to 1 dataunit/ms. The mean transmission lengths of the packets, $1/\mu_1 = 1/\mu_2 = 1$ ms.

Table 3-1. Optimal values of the mean transmission rates for a 2-link collision network for various values of sensing delays. The optimum values of the mean transmission rates are the solution to the constrained problem defined in (3-9), (3-14), and (3-15).

Sensing Delay	Max. Feasible Arrival Rate		Opt. Mean TX rate	
	λ_1	λ_2	R_1	R_2
0.001	0.4	0.6	4.15	6.22
0.01	0.39	0.42	6.05	6.49
0.1	0.2	0.39	1.33	2.35

A CSMA system with collisions is implemented in MATLAB. Fig. 3-4 shows the evolution of the queue lengths of the nodes 1 and 2 (refer to Fig. 3-1) for a sensing delay of $\delta T_s = 0.01$ ms. The optimal mean transmission rates ($R_1 = 6.05$ dataunits/ms, $R_2 = 6.49$ dataunits/ms) are generated by `fmincon`, and the stable arrival rates of $\lambda_1 = 0.16$ dataunits/ms and $\lambda_2 = 0.2$ dataunits/ms are used.

A 3-link collision network is simulated similarly, and the optimal values of the mean transmission rates, R_1, R_2 and R_3 , are obtained and tabulated as shown in Table 3-2 for different values of the sensing delay δT_s . Fig. 3-5 shows the evolution of queue lengths of the nodes 1, 2, and 3 (refer to Fig. 3-1) for a sensing delay of $\delta T_s = 0.01$ ms. The mean transmission lengths of the packets, $1/\mu_1 = 1/\mu_2 = 1/\mu_3 = 1$ ms. The optimal mean transmission rates ($R_1 = 6.54$ dataunits/ms, $R_2 = 10.19$ dataunits/ms, $R_3 = 11.49$ dataunits/ms) are generated by `fmincon`, and the stable arrival rates of $\lambda_1 = 0.01$ dataunits/ms, $\lambda_2 = 0.05$ dataunits/ms, $\lambda_3 = 0.02$ dataunits/ms are used.

The simulations are repeated 10 times for each of 2-link and 3-link collision networks, and the average (arithmetic mean) of the number of collisions is calculated for each case. Table 3-3 shows the average number of collisions when a set of optimized value of the mean transmission rates are used. The packet collisions in the network are reduced to less than 0.2% for the sensing delays listed in the table.

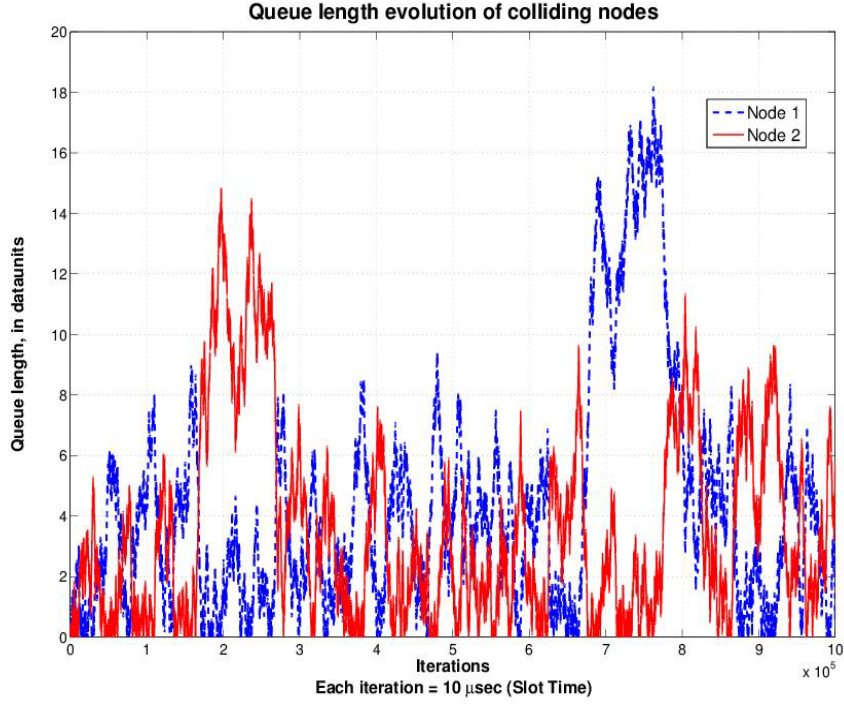


Figure 3-4. Queue lengths of nodes 1 and 2 transmitting to the same node 3. The optimum values of the mean transmission rates are the solution to the constrained problem defined in (3-9), (3-14), and (3-15). All nodes are in the sensing region. $\delta T_s = 0.01$ ms, $R_1 = 6.05$ dataunits/ms, $R_2 = 6.49$ dataunits/ms, $\lambda_1 = 0.16$ dataunits/ms, $\lambda_2 = 0.2$ dataunits/ms.

Table 3-2. Optimal values of the mean transmission rates for a 3-link collision network for various values of sensing delays. The optimum values of the mean transmission rates are the solution to the constrained problem defined in (3-9), (3-14), and (3-15).

Sensing Delay	Max. Feasible Arrival Rate			Opt. Mean TX rate		
	λ_1	λ_2	λ_3	R_1	R_2	R_3
0.001	0.22	0.31	0.3	7.31	10.28	9.95
0.01	0.13	0.21	0.24	6.54	10.19	11.49
0.1	0.12	0.12	0.1	2.26	2.26	1.94

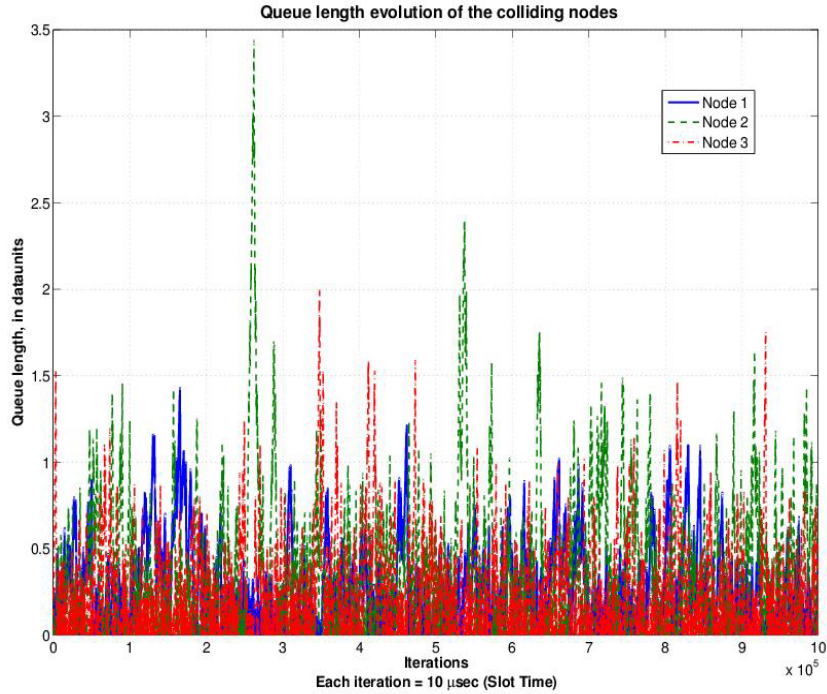


Figure 3-5. Queue lengths of nodes 1, 2, and 3 transmitting to the same node 4. The optimum values of the mean transmission rates are the solution to the constrained problem defined in (3-9), (3-14), and (3-15). All nodes are in the sensing region. $\delta T_s = 0.01$ ms, $R_1 = 6.54$ dataunits/ms, $R_2 = 10.19$ dataunits/ms, $R_3 = 11.49$ dataunits/ms, $\lambda_1 = 0.02$ dataunits/ms, $\lambda_2 = 0.05$ dataunits/ms, $\lambda_3 = 0.05$ dataunits/ms.

Table 3-3. Average number of collisions for a 2-link and 3-link collision networks for various values of sensing delays. The optimum values of the mean transmission rates are the solution to the constrained problem defined in (3-9), (3-14), and (3-15).

Sensing Delay, δT_s , in ms	Av. collisions using optimized Mean TX rates, in %	
	2-link	3-link
0.001	0.06	0.16
0.01	0.08	0.17
0.1	0.02	0.04

3.2 Throughput Maximization in CSMA Networks with Collisions and Hidden Terminals

Two sources of failure in the carrier-sensing mechanism are delays in the carrier sensing mechanism and hidden terminals, in which an ongoing transmission cannot be detected at a terminal that wishes to transmit because the path loss from the active transmitter is large. Collisions due to sensing delays was modeled in Section 3.1. In this section, the effect of these carrier-sensing failures (both due to sensing mechanism and hidden terminals) is modeled using a continuous-time Markov model. The throughput of the network is determined using the stationary distribution of the Markov model. The throughput is maximized by finding optimal mean transmission rates for the terminals in the network subject to constraints on successfully transmitting packets at a rate that is at least as great as the packet arrival rate.

3.2.1 Network Model

Consider an $(n + k)$ -link network with $n + k + 1$ nodes as shown in Fig. 3-6, where network A consists of n links and network B consists of k links. Assume that all nodes can sense all other nodes in the network. However, there is a sensing delay, so that if two nodes initiate packet transmission within a time duration of δT_s , there will be a collision. Let $(n + k)$ denote the total number of links in the network. In a typical CSMA network, the transmitter of node m backs off for a random period before it sends a packet to its destination node, if the channel is idle. If the channel is busy, the transmitter freezes its backoff counter until the channel is idle again. This backoff time, or the waiting time, for each link m is exponentially distributed with mean $1/R_m$. The objective in this chapter is to determine the optimal values of the mean transmission rates R_m , $m = 1, 2, \dots, n + k$, so that the throughput in the network is maximized. For this purpose, a Markovian model is used with states defined as $x^i : \mathcal{A} \rightarrow \{0, 1\}^{n+k}$, where $i \in \mathcal{A}$ represents the status of the network, which takes the value of 1 for an active link and 0 represents an idle link. For example, if the m th link in state i is active, then $x_m^i = 1$.

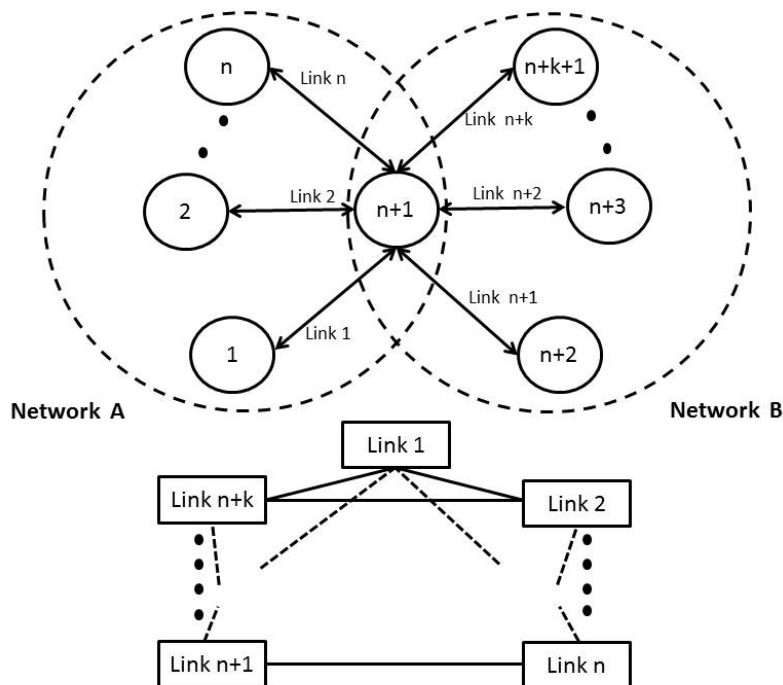


Figure 3-6. An $(n + k)$ -link network scenario and conflict graph.

Previous work assumes that the propagation delay between neighboring nodes is zero (cf. [31, 33]). Since propagation delays enable the potential for collisions, there exists motivation to maximize the throughput in the network in the presence of these delays. Additionally, collisions due to hidden terminals are possible, and this section captures the effect of hidden terminals in the CSMA Markov chain described in the following section.

3.2.2 CSMA Markov Chain

Formulations of Markov models for capturing the MAC layer dynamics in CSMA networks were developed in [31, 32]. The stationary distribution of the states and the balance equations were developed and used to quantify the throughput. Recently, a continuous time CSMA Markov model without collisions was used in [33] to develop an adaptive CSMA to maximize throughput. Collisions were introduced in [37] in the Markov model, and the mean transmission length of the packets are used as the control variable to maximize the throughput. Since most applications experience random length of packets,

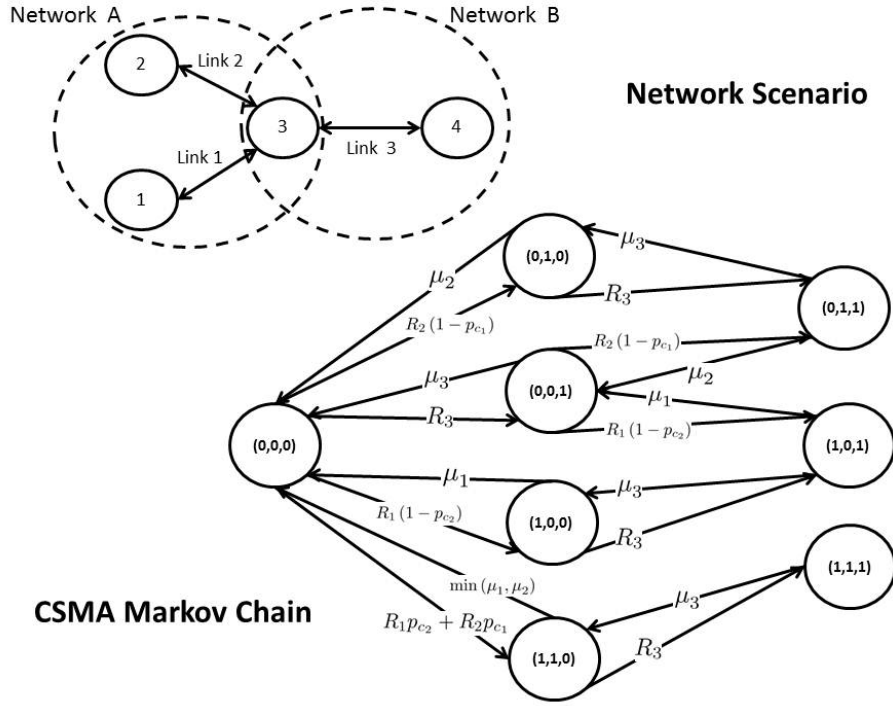


Figure 3-7. CSMA Markov chain with collision states for a 3-link network scenario with hidden terminals.

the transmission rates (packets/unit time), R_m , $m = 1, 2, \dots, n$, provide a practical measure.

The model for waiting times is based on the CSMA random access protocol. The probability density function of the waiting time T_m is given by (3-1). Due to the sensing delay experienced by the network nodes, the probability that link m becomes active within a time duration of δT_s from the instant link l becomes active is given in (3-2). Thus, the rate of transition G_i to one of the non-collision states in the Markov chain in Fig. 3-7 is as defined in (3-3). The rate of transition G_i to one of the collision states is given in (3-4). For example, the state (1, 1, 0) in Fig. 3-7 represents the collision state (for network A), which occurs when a link tries to transmit within a time span of δT_s from the instant another link starts transmitting.

The primary objective of modeling the network as a continuous CSMA Markov chain is that the probability of collision-free transmission needs to be maximized. For this purpose, the rate r_i is defined as

$$r_i \triangleq \begin{cases} \ln \left\{ \frac{\sum_{u=1}^n \left(x_u^i R_u \prod_{l \neq u} (1 - p_{c_l})^{(1-x_l^i)} \right)}{\sum_{u=1}^n x_u^i \mu_u} \right\}, & i \in \mathcal{A}_T \\ \frac{\sum_{u=1}^n \left(x_u^i R_u \prod_{l \neq u} (p_{c_l})^{x_l^i} (1 - p_{c_l})^{(1-x_l^i)} \right)}{\min_{m: x_m^i \neq 0} (\mu_m)}, & i \in \mathcal{A}_C \\ 1, & i \in \mathcal{A}_I, \end{cases} \quad (3-17)$$

so that the stationary distribution of the continuous time Markov chain can be defined as in (3-4) as

$$p(i) \triangleq \frac{\exp(r_i)}{\sum_j \exp(r_j)}, \quad (3-18)$$

where, in (3-17), $1/\mu_m$ is the mean transmission length of the packets if the network is in one of the states in set \mathcal{A}_T in sensing region A . The set $\mathcal{A}_T \triangleq \mathcal{A}_C^c \setminus (0,0)^T$ represents the set of all collision-free transmission states, where the elements in the set \mathcal{A}_C represents the collision states, and the elements in the set \mathcal{A}_C^c represents the non-collision states. The set \mathcal{A}_I represents the inactive state, i.e., $x^i = (0,0,0)$. In (3-17), the definitions for the rate of transitions in (3-3) and (3-4) are used, and (3-18) satisfies the detailed balance equation (cf. [78]).

In addition, if there are Hidden Terminals (HT) in the network as shown in Fig. 3-7, then r_i can be defined for the sensing region B in a similar way as defined for sensing region A in (3-17). Let sets \mathcal{B}_T , \mathcal{B}_C , and \mathcal{B}_I represent the collision-free transmission states, collision states, and the inactive states respectively. Based on the transmission, collision and idle states of the links in the sensing regions A and B , i belongs to one of the

combinations of the sets \mathcal{A}_T , \mathcal{A}_C , \mathcal{A}_I , \mathcal{B}_T , \mathcal{B}_C , and \mathcal{B}_I . Therefore (cf. [31]),

$$r_i \triangleq \begin{cases} F_A F_B, & i \in \mathcal{A}_T \cup \mathcal{B}_T \\ G_A F_B, & i \in \mathcal{A}_C \cup \mathcal{B}_T \\ F_B, & i \in \mathcal{A}_I \cup \mathcal{B}_T \\ F_A G_B, & i \in \mathcal{A}_T \cup \mathcal{B}_C \\ G_A G_B, & i \in \mathcal{A}_C \cup \mathcal{B}_C \\ G_B, & i \in \mathcal{A}_I \cup \mathcal{B}_C \\ F_A, & i \in \mathcal{A}_T \cup \mathcal{B}_I \\ G_A, & i \in \mathcal{A}_C \cup \mathcal{B}_I \\ 1, & i \in \mathcal{A}_I \cup \mathcal{B}_I, \end{cases}$$

where

$$F_A \triangleq \ln \left\{ \frac{\sum_{u=1}^n \left(x_u^i R_u \prod_{l \neq u} (1 - p_{cl})^{(1-x_l^i)} \right)}{\sum_{u=1}^n x_u^i \mu_u} \right\},$$

$$G_A \triangleq \frac{\sum_{u=1}^n \left(x_u^i R_u \prod_{l \neq k} (p_{cl})^{x_l^i} (1 - p_{cl})^{(1-x_l^i)} \right)}{\min_{m: x_m^i \neq 0} (\mu_m)}.$$

F_B and G_B can be defined similarly for network B in Fig. 3-6.

3.2.3 Throughput Maximization

To quantify the throughput, a log-likelihood function is defined as the summation over all the collision-free transmission states as

$$F(R) \triangleq \sum_{i \in (\mathcal{A}_T \cup \mathcal{B}_I) \cup (\mathcal{A}_I \cup \mathcal{B}_T)} \ln(p(i)). \quad (3-19)$$

By using the definition for $p(i)$ in (3-5), the log-likelihood function in (3-19) can be rewritten as

$$\begin{aligned}
F(R) = & \sum_{u=1}^n \ln \left(\exp \left(\ln \left(\frac{R_u}{\mu_u} \right) \right) \right) - (n-1) \sum_{u=1}^n R_u \delta T_s \\
& + \sum_{v=1+1}^{k+n} \ln \left(\exp \left(\ln \left(\frac{R_v}{\mu_v} \right) \right) \right) - (k-1) \sum_{v=n+1}^{k+n} R_v \delta T_s \\
& - (n+k) \ln \left[\sum_{i \in \mathcal{A}_T \cup \mathcal{B}_T} \exp(F_A F_B) + \sum_{i \in \mathcal{A}_C \cup \mathcal{B}_T} \exp(G_A F_B) \right. \\
& + \sum_{i \in \mathcal{A}_I \cup \mathcal{B}_T} \exp(F_B) + \sum_{i \in \mathcal{A}_T \cup \mathcal{B}_C} \exp(F_A G_B) \\
& + \sum_{i \in \mathcal{A}_C \cup \mathcal{B}_C} \exp(G_A G_B) + \sum_{i \in \mathcal{A}_I \cup \mathcal{B}_C} \exp(G_B) \\
& \left. + \sum_{i \in \mathcal{A}_T \cup \mathcal{B}_I} \exp(F_A) + \sum_{i \in \mathcal{A}_C \cup \mathcal{B}_I} \exp(G_A) + \sum_{i \in \mathcal{A}_I \cup \mathcal{B}_I} \exp(1) \right]. \quad (3-20)
\end{aligned}$$

The function $F(R)$ in (3-8) is concave, since natural logarithm and summation of concave functions is a concave function (cf. [79]). In addition, $F(R) \leq 0$ since $\ln(p(x^i)) \leq 0$ from the definition of $p(x^i)$ in (3-18). The optimization problem is defined as

$$\max_R (F(R)). \quad (3-21)$$

In addition to maximizing the log-likelihood function, certain constraints must be satisfied. The service rate $S(R)$ at each transmitter of a link needs to be equal to the arrival rate λ , and the chosen mean transmission rates R_k , $k = 1, 2, \dots, n$, need to be non-negative. Thus, the optimization problem can be formulated as

$$\max_R (F(R))$$

subject to

$$\ln \lambda - \ln S(R) = 0, \quad (3-22)$$

and

$$R \geq 0, \quad (3-23)$$

where $R \in \mathbb{R}^n$, $S(R) \in \mathbb{R}^{n-1}$, and $\lambda \in \mathbb{R}^{n-1}$. The service rate for a link is the rate at which a packet is transmitted, and is quantified for sensing region A as

$$S_m(R) \triangleq \frac{\exp\left(\ln\left(\frac{R_k \prod_{l \neq m} \exp(-R_l \delta T_s)}{\mu_m}\right)\right)}{\sum_j \exp(r_j)},$$

$m = 1, 2, \dots, n - 1$, and the denominator is defined in (3-17). Service rates for sensing region B can be defined similarly. Note that $\ln \lambda_m - \ln S_m(R) = 0$, and $\lambda_m > 0$ is concave for all m . The optimization problem defined above is a concave constrained nonlinear programming problem, and obtaining an analytical solution is difficult. There are numerical techniques adopted in the literature which have investigated such problems in detail [79–82]. As detailed in Section 3.2.4, a suitable numerical optimization algorithm is employed to solve the optimization problem defined in (3-21)-(3-23).

3.2.4 Simulation Results

The constrained concave nonlinear programming problem defined in (3-21)-(3-23) is solved by optimizing the mean transmission rates R_m , $m = 1, 2, \dots, n + k$, of the transmitting nodes in the network of Fig. 3-6. A MATLAB built-in function `fmincon` is used to solve the optimization problem by configuring it to use the interior point algorithm (cf. [83, 84]).

Once the mean transmission rates are optimized, they are fixed in a simulation (developed in MATLAB) that uses the CSMA MAC protocol. The function `fmincon` solves the optimization problem only for a set of feasible arrival rates. A slot time of $10 \mu s$ is used, and the mean transmission lengths of the packets, $1/\mu_m$, $m = 1, 2, \dots, n + k$, are set to 1 ms. Further, a stable (and feasible) set of arrival rates, in the sense that the queue lengths at the transmitting nodes are stable, are chosen before the simulation.

The collision network of Fig. 3-6 is simulated using the platform explained above. The optimal values of the mean transmission rates, R_1 , R_2 , and R_3 , are obtained and tabulated as shown in Table 3-4 for different values of the sensing delay δT_s (Note that

Table 3-4. Optimal values of the mean transmission rates for a 3-link collision network with hidden terminals (refer to Fig. 3-7) for various values of sensing delays. The optimum values of the mean transmission rates are the solution to the constrained problem defined in (3-21)-(3-23).

Sensing Delay	Max. Feasible Arrival Rate			Opt. Mean TX rate		
	λ_1	λ_2	λ_3	R_1	R_2	R_3
	0.001	0.2	0.2	0.1	3.94	3.94
0.01	0.18	0.17	0.11	3.78	3.58	2.23
0.1	0.12	0.12	0.1	2.56	2.56	1.65

in the scenario of Fig. 3-6, the sensing delay applies to the nodes in network A). The capacity of the channel is normalized to 1 dataunit/ms. The mean transmission lengths of the packets are $1/\mu_1 = 1/\mu_2 = 1/\mu_3 = 1$ ms.

A simulation of a CSMA system with collisions is implemented in MATLAB. Fig. 3-8 shows the evolution of the queue lengths of nodes 1, 2, and 4 (refer to Fig. 3-6) for a sensing delay of $\delta T_s = 0.01$ ms. The optimal mean transmission rates ($R_1 = 3.78$ dataunits/ms, $R_2 = 3.58$ dataunits/ms, $R_3 = 2.23$ dataunits/ms) are generated by `fmincon`, and the stable arrival rates of $\lambda_1 = 0.05$ dataunits/ms, $\lambda_2 = 0.05$ dataunits/ms, and $\lambda_3 = 0.01$ dataunits/ms are used.

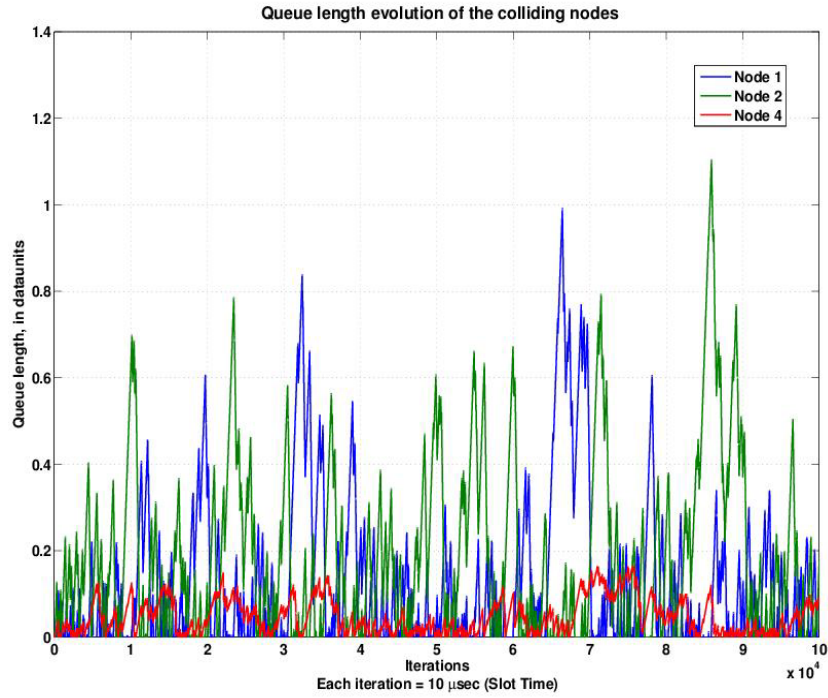


Figure 3-8. Queue lengths of nodes 1, 2, and 4 transmitting to the same node 3. The optimum values of the mean transmission rates are the solution to the constrained problem defined in (3-21)-(3-23). All nodes are in the sensing region, and $\delta T_s = 0.01$ ms, $R_1 = 3.78$ dataunits/ms, $R_2 = 3.58$ dataunits/ms, $R_3 = 2.23$ dataunits/ms, $\lambda_1 = 0.02$ dataunits/ms, $\lambda_2 = 0.05$ dataunits/ms, $\lambda_3 = 0.05$ dataunits/ms.

CHAPTER 4

CONGESTION CONTROL FOR DIFFERENTIATED-SERVICES NETWORKS WITH ARRIVAL-RATE DELAYS

Network packet traffic in the transport layer plays a vital role in affecting the throughput of Internet-style networks. Common queue length management techniques on nodes in such networks focus on servicing the packets based on their Quality of Service (QoS) requirements (e.g., Differentiated-Services, or DiffServ, networks). In this chapter, continuous control strategies are suggested for a DiffServ network to track the desired ensemble average queue lengths in multiple queues. A Lyapunov-based stability analysis is provided to illustrate global asymptotic regulation of the ensemble average queue length of the Premium Service buffer. In addition, arrival rate delays due to propagation and processing that affects the control input of the Ordinary Service buffer are addressed, and a Lyapunov-based stability analysis is provided to illustrate global asymptotic regulation of the ensemble average queue length of this service. Simulations demonstrate the performance and feasibility of the controller, along with showing global asymptotic regulation close to the desired values of the queue lengths in the Premium Service and Ordinary Service buffers.

4.1 Queuing System Model

DiffServ architectures are examples of high-speed network architectures used in TCP/IP and ATM technologies. In [56], inspired by [43], the incoming traffic to a node in a network is classified into Premium Traffic Service, Ordinary Traffic Service, and Best Effort Traffic Service. Premium Traffic Service is designed for applications such as video conferencing, audio, and video on demand, which are characterized by stringent loss and delay constraints. Ordinary Traffic Service have some flexibility in terms of delay requirements. Examples of such applications include web browsing, email, and ftp. Finally, Best Effort Traffic Service are designed for the class of applications that do not have any delay or loss constraints. In this chapter, the control objective is defined for applications that use Premium Traffic Service and Ordinary Traffic Service (refer to Fig. 4-1).

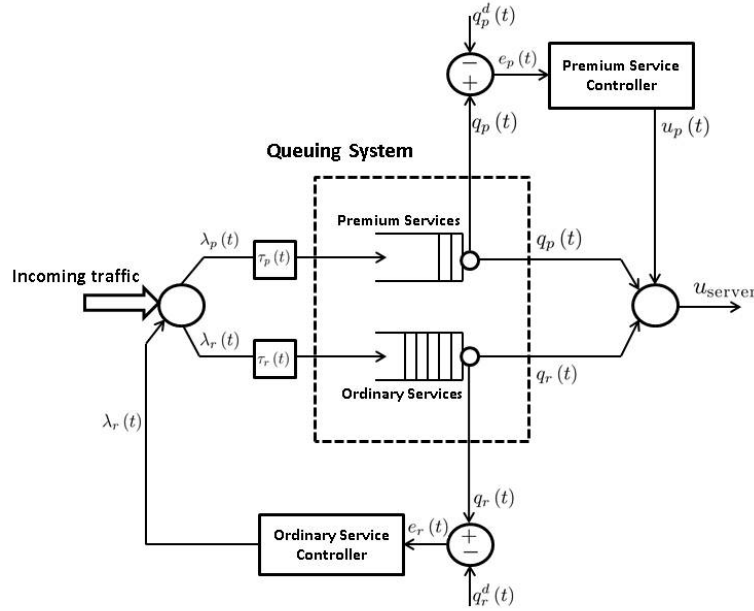


Figure 4-1. Schematic of a DiffServ Queuing System.

The subsequent development is based on a Fluid Flow Model (FFM) commonly used in network performance analysis (cf. [41, 44]). Such models are general, and describe a wide range of queueing and contention systems (cf. [85–87]). Assuming no packet drops, the flow conservation principle for a single queue (cf. [41, 56]) is used to define the evolution of the ensemble average of the queue length, $q(t) \in \mathbb{R}^+$, in the system as

$$\dot{q} = -uG(q) + \lambda, \quad (4-1)$$

where $q(0) = q_0$, and $G : \mathbb{R}^+ \rightarrow [0, 1)$ is the offered load, also known as the ensemble average utilization of the queue at time t , and the control input $u(t) \in \mathbb{R}^+$ is the queue server capacity. In (4-1), $\lambda(t) \in \mathbb{R}^+$ is the ensemble average arrival rate defined as

$$\lambda(t) = \mathbb{E}[a],$$

where $\mathbb{E}[a]$ denotes the expected value of the arrival rate, $a(t) \in \mathbb{R}^+$. The queueing model based on [56] uses M/M/1 (i.e., Markovian input, Markovian output, single server) assumptions (cf. [41, 44]) to obtain the ensemble average queue length evolution. In addition, the presence of possible delays (cf. [88–90]) in the arrival rates to the Premium Service, and more critically the Ordinary Service buffers will affect the control significantly. Such delays arise due to processing and propagation (for instance, the IDCC scheme in [56] can potentially cause delays). In this work, we address time-varying arrival rate delays; hence, the ensemble average queue length evolution can be expressed as

$$\dot{q}_i = -u_i \left(\frac{q_i}{1 + q_i} \right) + \lambda_i(t - \tau_i(t)), \quad (4-2)$$

where $i \in \{p, r\}$ and subscripts p and r represent Premium Service and Ordinary Service respectively. It is assumed that $0 \leq \tau_r(t) \leq \tau_{r\max}$, and $|\dot{\tau}_r(t)| \leq \tau_{r\max}^d < 1$, where $\tau_{r\max}$ and $\tau_{r\max}^d$ are known positive constants. The assumption for $\dot{\tau}_r(t)$ indicates that the time-delay must be slowly time-varying. It is also assumed that $|\dot{\tau}_p(t)| \leq \tau_{p\max}^d$ and $|\ddot{\tau}_p(t)| \leq \tau_{p\max}^d$, where $\tau_{p\max}$ and $\tau_{p\max}^d$ are known positive constants. The model in (4–2) is valid for $0 \leq q_i(t) \leq q_{\text{buffer size}}$ and $0 \leq u(t) \leq u_{\text{server}}$, where $q_{\text{buffer size}}$ is the maximum possible queue size, and u_{server} is the maximum allowable server rate.

4.2 Premium Service

The unknown average arrival rate of the Poisson arrival process is denoted by $\lambda_p^a(t) \triangleq \lambda_p(t - \tau_p(t)) \in \mathbb{R}^+$, and $u_p(t) \in \mathbb{R}^+$ is the queue server capacity that acts as the control variable. It is assumed that $\forall t$, $\lambda_p^a(t)$ is upper bounded by the allowable rate for incoming Premium Traffic, denoted by $\lambda_{p\max}^a$, which in-turn is bounded by u_{server} [56]. In addition to $\lambda_p(t)$ being bounded, its first and second derivatives are assumed to be bounded [56]. Since $\dot{\tau}_p(t)$ and $\ddot{\tau}_p(t)$ are assumed to be bounded, the first and second time derivatives of $\lambda_p^a(t)$ can be bounded from its definition as

$$\left| \dot{\lambda}_p^a \right| \leq \zeta_{\dot{\lambda}_p^a}, \quad \left| \ddot{\lambda}_p^a \right| \leq \zeta_{\ddot{\lambda}_p^a}. \quad (4-3)$$

4.2.1 Control Design

To facilitate the subsequent analysis of the queueing system, an ensemble average queue length error $e_p(t) \in \mathbb{R}$ is defined as

$$e_p \triangleq q_p - q_{p_d}, \quad (4-4)$$

where $q_{p_d}(t) \in \mathbb{R}$ is the desired ensemble average queue length provided by the network operator. It is assumed that the first and second derivatives of the desired ensemble average queue length are known and bounded [56]. To facilitate the subsequent analysis, a filtered tracking error is defined as

$$r_p \triangleq \dot{e}_p + \alpha_p e_p, \quad (4-5)$$

where $\alpha_p \in \mathbb{R}^+$ denotes a constant control gain. The filtered tracking error is only introduced to facilitate the subsequent analysis and is not assumed to be measurable. Taking the time derivative of (4-4) and using (4-5) yields

$$\begin{aligned} r_p &= \dot{q}_p - \dot{q}_{p_d} + \alpha e_p \\ &= -u_p \left(\frac{q_p}{1 + q_p} \right) + \lambda_p^a(t) - \dot{q}_{p_d} + \alpha e_p. \end{aligned} \quad (4-6)$$

From M/M/1 queueing formulas, the ensemble average utilization of the queue is defined as $G(q_p) \triangleq q_p / (1 + q_p)$ and is assumed to be known (cf. [56, 57]). Hence, the control law for premium service is defined as

$$u_p \triangleq \left(\frac{q_p}{1 + q_p} \right)^{-1} \mu, \quad (4-7)$$

where $\mu(t)$ is a subsequently designed auxiliary controller. After substituting (4-7) into (4-6), the filtered tracking error can be rewritten as

$$r_p = -\mu + \lambda_p^a(t) - \dot{q}_{p_d} + \alpha e_p. \quad (4-8)$$

To facilitate the design of $\mu(t)$, the time derivative of (4–8) is obtained as

$$\dot{r}_p = -\dot{\mu} + \dot{\lambda}_p^a(t) - \ddot{q}_{pd} + \alpha \dot{e}_p. \quad (4-9)$$

Based on (4–9) and the subsequent stability analysis, the auxiliary control term $\mu(t)$ is defined as

$$\mu \triangleq \dot{q}_{pd}(0) - \dot{q}_{pd}(t) + \nu, \quad (4-10)$$

where $\nu(e_p) \in \mathbb{R}$ is the Filippov solution to the following differential equation

$$\dot{\nu} = (k_{p1} + k_{p2} + \alpha_p) r_p + \beta \text{sgn}(e_p) + e_p, \quad \nu(0) = 0, \quad (4-11)$$

where $k_p, \beta \in \mathbb{R}^+$ are constant control gains. The existence of solutions can be established using Filippov theory of differential inclusions (cf. [91–94]) for $\dot{\nu} \in K[h](e_p, r_p, t)$ where $h(e_p, r_p, t) \in \mathbb{R}$ is defined in the right-hand side of $\dot{\nu}$ in (4–11), and

$$K[h] \triangleq \bigcap_{\delta > 0} \bigcap_{\mu S_m = 0} \mathbf{co} h(B(v, \delta) - S_m),$$

where $\bigcap_{\mu S_m = 0}$ denotes the intersection of all sets S_m of Lebesgue measure zero, \mathbf{co} denotes convex closure, and $B(v, \delta)$ denotes the open ball of radius δ around v .

The closed-loop error system is obtained by substituting the time derivative of (4–10) into (4–9) as

$$\dot{r}_p = \dot{\lambda}_p^a(t) - ((k_{p1} + k_{p2} + \alpha_p) r_p + \beta \text{sgn}(e_p) + e_p) + \alpha \dot{e}_p. \quad (4-12)$$

4.2.2 Stability Analysis

Theorem 4.1: The controller designed in (4–7) and (4–11) ensures global asymptotic ensemble average queue length regulation in the Premium Service buffer provided the control gains are selected according to the sufficient conditions

$$k_{p2} > \frac{\alpha_p^2}{2}, \quad \alpha_p < 2, \quad (4-13)$$

and

$$\beta > \zeta_{\dot{\lambda}_p^a} + \frac{1}{\alpha} \zeta_{\ddot{\lambda}_p^a}, \quad (4-14)$$

where $\zeta_{\dot{\lambda}_p^a}$ and $\zeta_{\ddot{\lambda}_p^a}$ are introduced in (4-3).

Proof. Let $y_p(t) \in \mathbb{R}^3$ be defined as $y_p(t) \triangleq \begin{bmatrix} z_p^T(t) & \sqrt{P} \end{bmatrix}^T$ where $z_p(t) \in \mathbb{R}^2$ is defined as $z_p(t) \triangleq \begin{bmatrix} e_p(t) & r_p(t) \end{bmatrix}^T$, and the auxiliary function $P(e_p, t) \in \mathbb{R}$ is the Filippov solution to the following differential equation

$$\dot{P}(t) = -r_p \left(\dot{\lambda}_p^a - \beta \operatorname{sgn}(e_p) \right), \quad (4-15)$$

$$P(e_p(t_0), t_0) = \beta |e_p(0)| - e_p(0) \dot{\lambda}_p^a(0). \quad (4-16)$$

Existence of solutions for $P(e_p, t)$ can be established using Filippov theory of differential inclusions in a manner similar to the development in (4-11). Provided the sufficient condition in (4-14) is satisfied, the condition that $P(t) \geq 0$ can be proven (refer to Appendix C). Let $V_a(y_p, t) : \mathbb{R}^3 \times [0, \infty) \rightarrow \mathbb{R}$ be a regular and a continuously differentiable function in y_p , defined as

$$V_a(y_p, t) = \frac{1}{2} r_p^2 + \frac{1}{2} e_p^2 + P. \quad (4-17)$$

The time derivative of (4-17) exists almost everywhere (a.e.), i.e., for almost all $t \in [t_0, t_f]$, and $\dot{V}_a(y_p, t) \stackrel{a.e.}{\in} V_p(y_p, t)$, where

$$\dot{V}_p(y_p, t) = \bigcap_{\xi \in \partial V_p(y_p, t)} \xi^T K \begin{bmatrix} \dot{e}_p & \dot{r}_p & \frac{1}{2} P^{-\frac{1}{2}} \dot{P} \end{bmatrix},$$

where $\partial V_p(y_p)$ is the generalized gradient of $V_p(y_p, t)$ [95]. Since $V_p(y_p, t)$ is a continuously differentiable function in y_p ,

$$\dot{V}_p \subset \nabla V_p K [\cdot]^T, \quad (4-18)$$

where

$$\nabla V_p = \begin{bmatrix} e_p & r_p & 2\sqrt{P} \end{bmatrix}.$$

Using the calculus of $K[\cdot]$ from [96] and by using (4-12) and (4-15), (4-15) can be expressed as

$$\begin{aligned} \dot{\hat{V}}_p \subset & r_p \left\{ \dot{\lambda}_p^a - (k_{p1} + k_{p2} + \alpha_p) r_p - \beta K[\text{sgn}(e_p)] - e_p + \alpha_p \dot{e}_p \right\} \\ & + e_p \{r_p - \alpha_p e_p\} - r_p \left(\dot{\lambda}_p^a - \beta K[\text{sgn}(e_p)] \right), \end{aligned} \quad (4-19)$$

where $K[\text{sgn}(e_p)] = \Psi(e_p)$ [96] such that

$$\Psi(e_p) = \begin{cases} 1, & \text{if } e_p(t) > 0 \\ [-1, 1], & \text{if } e_p(t) = 0 \\ -1, & \text{if } e_p(t) < 0. \end{cases}$$

Using (4-5), (4-19) can be rewritten as

$$\begin{aligned} \dot{\hat{V}}_p \stackrel{a.e.}{\leq} & -k_{p1} |r_p|^2 - k_{p2} |r_p|^2 - \alpha_p |r_p|^2 + \alpha_p r_p \{r_p - \alpha_p e_p\} \\ & - \alpha_p |e_p|^2, \end{aligned} \quad (4-20)$$

where the set in (4-19) reduces to the scalar inequality in (4-20) since the RHS is continuous a.e., i.e., the RHS is continuous except for the Lebesgue negligible set of times when $e_p = 0$ [97, 98]. Applying Young's Inequality, (4-20) can be rewritten as

$$\begin{aligned} \dot{\hat{V}}_p \stackrel{a.e.}{\leq} & -k_{p1} |r_p|^2 - k_{p2} |r_p|^2 - \alpha_p |r_p|^2 + \alpha_p |r_p|^2 + \frac{\alpha_p^2}{2} |e_p|^2 \\ & + \frac{\alpha_p^2}{2} |r_p|^2 - \alpha_p |e_p|^2. \\ \dot{\hat{V}}_p \stackrel{a.e.}{\leq} & -k_{p1} |r_p|^2 - \left(k_{p2} - \frac{\alpha_p^2}{2} \right) |r_p|^2 - \left(\alpha_p - \frac{\alpha_p^2}{2} \right) |e_p|^2. \end{aligned}$$

If the condition in (4-13) is satisfied

$$\dot{\hat{V}}_p \stackrel{a.e.}{\leq} -W_p(y_p), \quad (4-21)$$

where $W_p(y_p) \triangleq \sigma_p \|z_p\|^2$ where $\sigma_p \triangleq \min \left\{ k_{p1}, \left(k_{p2} - \frac{\alpha_p^2}{2} \right), \left(\alpha_p - \frac{\alpha_p^2}{2} \right) \right\}$. Since $e_p(t)$, $r_p(t) \in \mathcal{L}_\infty$, standard linear analysis methods can be used to prove that $\dot{e}_p(t) \in \mathcal{L}_\infty$ from (4-5). Since $e_p(t)$, $r_p(t) \in \mathcal{L}_\infty$, the assumption that $q_{pd}(t)$, $\dot{q}_{pd}(t)$ exist and are

bounded can be used along with (4-4) and (4-5) to conclude that $q_p(t), \dot{q}_p(t) \in \mathcal{L}_\infty$. Therefore, from (4-7) and (4-10), $u_p(t), \mu(t) \in \mathcal{L}_\infty$. Since $e_p(t), r_p(t), \dot{e}_p(t), \dot{\lambda}_p^a(t) \in \mathcal{L}_\infty$, (4-12) indicates that $\dot{r}_p(t) \in \mathcal{L}_\infty$. The definition of $W_p(y)$ and $z_p(t)$ can be used to prove that $W_p(y)$ is uniformly continuous. Therefore, Barbalat's lemma [99] can be invoked to conclude that

$$\|z_p(t)\|^2 \rightarrow 0 \quad \text{as } t \rightarrow \infty. \quad (4-22)$$

From the definition of $z_p(t)$, (4-22) can be used to show that

$$r_p(t) \rightarrow 0 \quad \text{and} \quad e_p(t) \rightarrow 0 \quad \text{as } t \rightarrow \infty.$$

□

4.3 Ordinary Service

The evolution of the ensemble average queue length for the Ordinary Service is given in (4-2) with $i = r$, i.e.,

$$\dot{q}_r = -u_r \left(\frac{q_r}{1 + q_r} \right) + \lambda_r(t - \tau_r(t)), \quad (4-23)$$

where

$$u_r(t) = u_{\text{server}} - u_p(t)$$

is known, and the control variable (ensemble average arrival rate) $\lambda_r(t - \tau_r(t)) \in \mathbb{R}$ needs to be designed. Let the ensemble average queue length error for the Ordinary Service queueing system $e_r(t) \in \mathbb{R}$ be defined as

$$e_r \triangleq q_r - q_{r_d}, \quad (4-24)$$

where $q_{r_d}(t) \in \mathbb{R}$ is the desired ensemble average queue length for this service. To facilitate the subsequent analysis, the filtered tracking error $r_r(t)$ is defined as

$$r_r \triangleq \dot{e}_r + \alpha_r e_r + \lambda_r(t) - \lambda_r(t - \tau_r(t)). \quad (4-25)$$

Based on the subsequent stability analysis, the controller for Ordinary Service, i.e., $\lambda_r(t)$, is designed as

$$\begin{aligned} \lambda_r(t) \triangleq & -k_r \left\{ \left(1 + \frac{\alpha_r}{k_r}\right) e_r + \int_0^t \left[\left(\alpha_r + \frac{1}{k_r}\right) e_r(\theta) + \lambda_r(\theta) - \lambda_r(t - \tau_r(\theta)) \right] d\theta \right\} \\ & + u_r \left(\frac{q_r}{1 + q_r} \right) + \dot{q}_{r_d} + k_r \left(1 + \frac{\alpha_r}{k_r}\right) e_r(0) \\ & - u_r(0) \left(\frac{q_r(0)}{1 + q_r(0)} \right) - \dot{q}_{r_d}(0). \end{aligned} \quad (4-26)$$

After taking the derivative of (4-24), using (4-23), and substituting for \dot{e}_r in (4-25) yields

$$r_r = -u_r \left(\frac{q_r}{1 + q_r} \right) - \dot{q}_{r_d} + \alpha_r e_r + \lambda_r(t). \quad (4-27)$$

An additional derivative of (4-27) is taken to facilitate the subsequent analysis. Hence, by using (4-26), the derivative of (4-27) can be expressed as

$$\begin{aligned} \dot{r}_r &= \frac{d}{dt} \left[-u_r \left(\frac{q_r}{1 + q_r} \right) \right] - \ddot{q}_{r_d} + \alpha_r \dot{e}_r - k_r [\dot{e}_r + \alpha_r e_r + \lambda_r(t) - \lambda_r(t - \tau_r(t))] \\ &+ \frac{d}{dt} \left[u_r \left(\frac{q_r}{1 + q_r} \right) \right] + \ddot{q}_{r_d} - \alpha_r \dot{e}_r - e_r. \\ &= -k_r r_r - e_r. \end{aligned} \quad (4-28)$$

4.3.1 Stability Analysis

Theorem 4.2: The controller designed in (4-26) ensures global asymptotic ensemble average queue length regulation in the Ordinary Service buffer provided the control gains are selected according to the sufficient conditions

$$\alpha_r > \frac{1}{2}, \quad \frac{2\omega(1 - \dot{\tau}_r)}{2\omega + 1} > \tau_r, \quad (4-29)$$

where $\omega \in \mathbb{R}^+$ is a subsequently defined control gain.

Proof: Let $y_r(t) \in \mathbb{R}^3$ be defined as $y_r(t) \triangleq \begin{bmatrix} z_r^T(t) & \sqrt{Q} \end{bmatrix}^T$ where $z_r(t) \in \mathbb{R}^2$ is defined as $z_r(t) \triangleq \begin{bmatrix} e_r(t) & r_r(t) \end{bmatrix}^T$. Let $Q(\dot{\lambda}_r, t, \tau_r) \in \mathbb{R}$ denote the Lyapunov-Krasovskii

functional, defined as

$$Q \triangleq \omega \int_{t-\tau_r(t)}^t \left(\int_s^t |\dot{\lambda}_r(\theta)|^2 d\theta \right) ds, \quad (4-30)$$

where $\omega \in \mathbb{R}^+$ is a known positive constant. Let $V_r(y_r, t) : \mathbb{R}^3 \times [0, \infty) \rightarrow \mathbb{R}$ be a positive-definite function defined as

$$V_r = \frac{1}{2}e_r^2 + \frac{1}{2}r_r^2 + Q. \quad (4-31)$$

Taking the derivative of (4-31), and using (4-25), (4-28) and (4-30) yields

$$\dot{V}_r = e_r(r_r - \alpha_r e_r - e_a) + r_r(-k_r r_r - e_r) + \omega \tau_r |\dot{\lambda}_r|^2 - \omega(1 - \dot{\tau}_r) \int_{t-\tau_r(t)}^t |\dot{\lambda}_r(\theta)|^2 d\theta, \quad (4-32)$$

where

$$e_a \triangleq \lambda_r(t) - \lambda_r(t - \tau_r(\theta)) = \int_{t-\tau_r(t)}^t \dot{\lambda}_r(\theta) d\theta.$$

Using Young's inequality,

$$|e_r| |e_a| \leq \frac{|e_r|^2}{2} + \frac{|e_a|^2}{2}. \quad (4-33)$$

Using (4-33) and by utilizing the fact that

$$|\dot{\lambda}_r(t)|^2 \leq \int_{t-\tau_r(t)}^t |\dot{\lambda}_r(\theta)|^2 d\theta, \quad |e_a|^2 \leq \tau_r \int_{t-\tau_r(t)}^t |\dot{\lambda}_r(\theta)|^2 d\theta,$$

the expression in (4-32) can be upper bounded as

$$\begin{aligned} \dot{V}_r &\leq -\alpha_r |e_r|^2 - k_r |r_r|^2 + \frac{|e_r|^2}{2} + \frac{\tau_r}{2} \int_{t-\tau_r(t)}^t |\dot{\lambda}_r(\theta)|^2 d\theta + \omega \tau_r \int_{t-\tau_r(t)}^t |\dot{\lambda}_r(\theta)|^2 d\theta \\ &\quad - \omega(1 - \dot{\tau}_r) \int_{t-\tau_r(t)}^t |\dot{\lambda}_r(\theta)|^2 d\theta \\ &= -\left(\alpha_r - \frac{1}{2}\right) |e_r|^2 - k_r |r_r|^2 - \left(\omega(1 - \dot{\tau}_r) - \omega \tau_r - \frac{\tau_r}{2}\right) \int_{t-\tau_r(t)}^t |\dot{\lambda}_r(\theta)|^2 d\theta. \end{aligned}$$

If (4-29) is satisfied, then

$$\dot{V}_r \leq -W_r(y_r), \quad (4-34)$$

where $W_r(y_r) \triangleq \sigma_r \|z_r\|^2$, for some positive constant $\sigma_r \in \mathbb{R}^+$. The inequality in (4-34) can be used to show that $e_r(t), r_r(t) \in \mathcal{L}_\infty$. The closed-loop error system can be used to show that the remaining signals are bounded. The definition of $W_r(y)$ and $z_r(t)$ can be used to prove that $W_r(y)$ is uniformly continuous. Therefore, Barbalat's lemma [99] can be invoked to conclude that

$$\|z_r(t)\|^2 \rightarrow 0 \quad \text{as } t \rightarrow \infty. \quad (4-35)$$

From the definition of $z_r(t)$, (4-35) can be used to show that

$$r_r(t) \rightarrow 0 \quad \text{and} \quad e_r(t) \rightarrow 0 \quad \text{as } t \rightarrow \infty.$$

4.4 Simulation Results

Numerical simulations are performed in Matlab to demonstrate the performance of the developed controller for the DiffServ network. Since the model in (4-2) is valid for $0 \leq u(t) \leq u_{\text{server}}$, the controllers implemented in the simulations for the Premium Service and Ordinary Service are

$$u_p(t) \triangleq \max \left[0, \min \left\{ u_{\text{server}}, \left(\frac{q_p}{1 + q_p} \right)^{-1} \mu \right\} \right] \quad (4-36)$$

and

$$u_r(t) = \max [0, u_{\text{server}} - u_p(t)], \quad (4-37)$$

respectively. Hence, the initial parameters are chosen appropriately based on the domain of operation of the DiffServ system. The maximum allowable server rate, u_{server} , is chosen to be 200 dataunits per unit time, where 1 unit time is equal to 100 ms. Initial ensemble average queue length for both the Premium Service, $q_p(0)$, and the Ordinary Service, $q_r(0)$, are chosen to be 100 dataunits. The initial server rate for Premium Service, $u_p(0)$, and the initial auxiliary control, $\mu(0)$, are both chosen to be 50 dataunits per unit time.

From (4-37), $u_r(0) = 950$ dataunits per unit time. The ensemble average arrival rate for Ordinary Service, $\lambda_r(0)$, is chosen to be 100 dataunits per unit time.

The desired ensemble average queue length for Premium, $q_{d_p}(t)$, and Ordinary Service, $q_{d_r}(t)$, are chosen to be 100 and 50 dataunits respectively. The arrival rate at the input of the Premium Service queue is chosen as

$$\lambda_p(t) = 30 + 0.05 \cos\left(\frac{\pi}{5}t\right) \text{ dataunits/unit time.}$$

The control gains are chosen as

$$k_{p_1} = 0.05, \quad k_{p_2} = 0.05, \quad \alpha_p = 0.501, \quad \beta = 0.1$$

for Premium Service, and

$$k_r = 0.1$$

for Ordinary Service. The Ordinary Service controller uses the technique of feedback linearization without arrival-rate delays (see [100]). The implemented controller for Premium Service is obtained by using (4-11) and substituting (4-10) into (4-36). Fig. 4-2 shows the ensemble average queue length plot and the corresponding server rates for Premium Services without arrival-rate delays. The queue length for Premium Service asymptotically converges close to the desired value as shown in Fig. 4-2.

Fig. 4-3 shows the ensemble average queue length plot and the corresponding average arrival rates for Ordinary Services without arrival-rate delays. The queue length error for Ordinary Service exponentially converges to zero.

With delays, the ensemble average queue length plot and the corresponding server rates for Premium Services is shown in Fig. 4-4 with a time-varying delay

$$\tau_p(t) = 0.5 + 0.1 \sin\left(\frac{\pi}{2}t\right) \text{ seconds.}$$

It can be inferred from Fig. 4-2 and Fig. 4-4 that the arrival-delay delay acts as a disturbance for Premium Service buffer, and hence the convergence of the ensemble

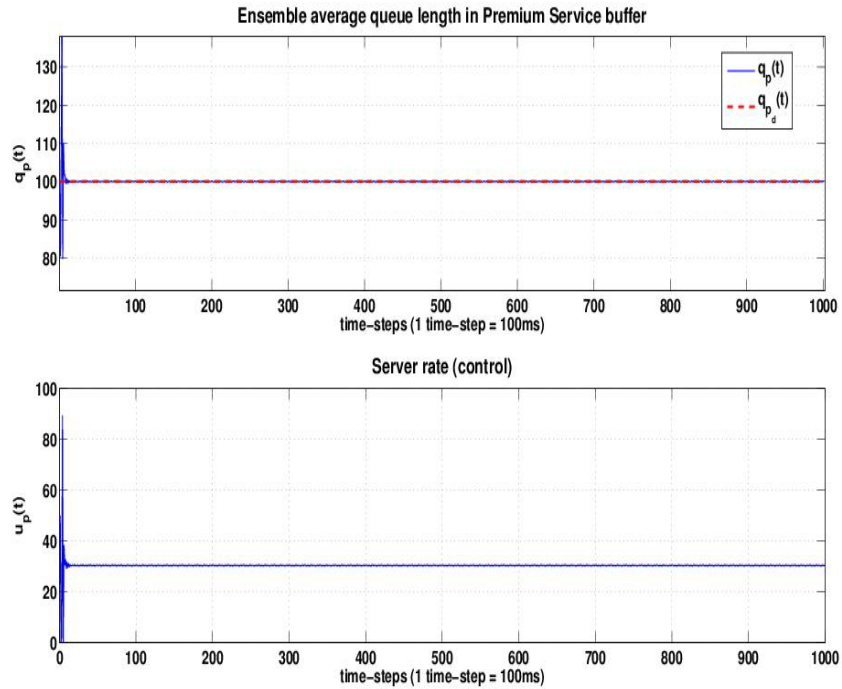


Figure 4-2. Ensemble average queue length and service rates for Premium Service without arrival-rate delays.

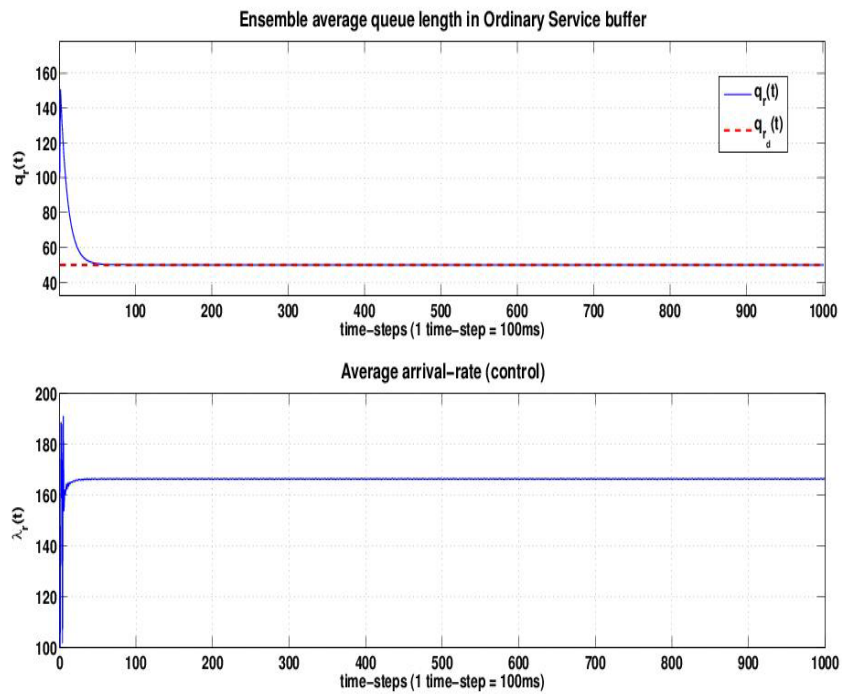


Figure 4-3. Ensemble average queue length and average arrival rates for Ordinary Service without arrival-rate delays.

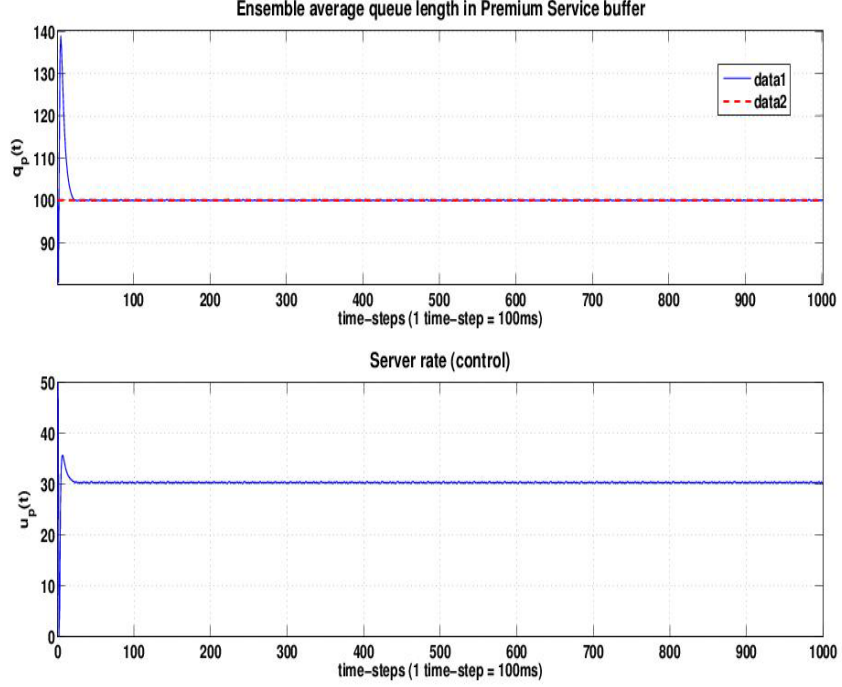


Figure 4-4. Ensemble average queue length and service rates for Premium Service with average arrival-rate delay.

average queue length in the Premium Service buffer without delay is similar to the convergence with delay, provided the delay bounds established in Section 4.1 are satisfied.

The ensemble average queue length in Ordinary Service buffer asymptotically converges close to zero with arrival-rate delay, unlike the case with no delay where we obtain exponential convergence (see Fig. 4-3). The control gains are chosen as

$$k_{p_1} = 0.5, \quad k_{p_2} = 0.12, \quad \alpha_p = 0.15, \quad \beta = 0.1$$

for Premium Service, and

$$k_r = 0.3, \quad \alpha_r = 0.01$$

for Ordinary Service. Fig. 4-5 shows the ensemble average queue length plot and the corresponding average arrival rate plot for Ordinary Service with time-varying delay,

$$\tau_r(t) = 0.1 + 0.1 \sin\left(\frac{\pi}{2}t\right) \text{ seconds.}$$

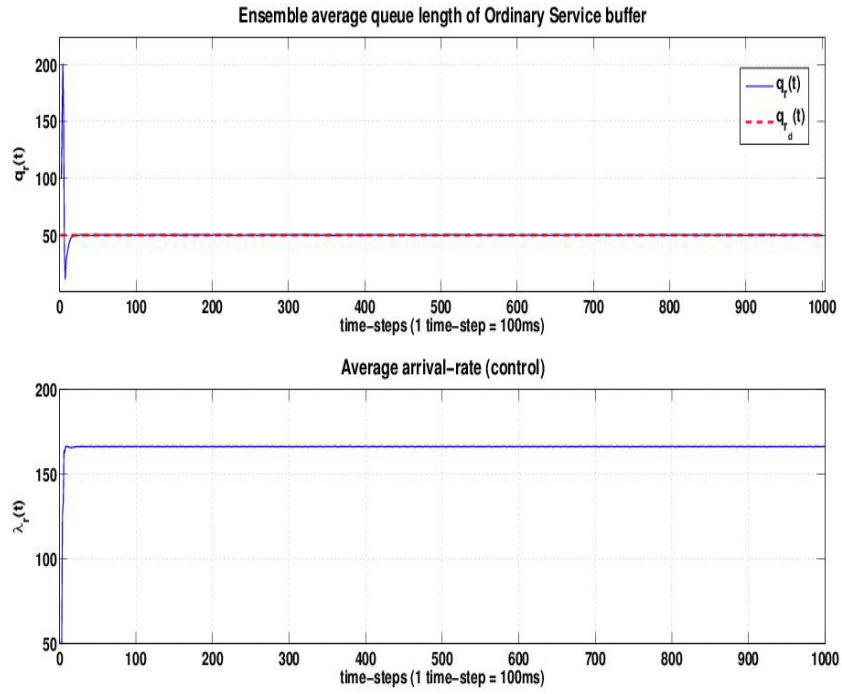


Figure 4-5. Ensemble average queue length and average arrival-rate for Ordinary Service with average arrival-rate delay.

CHAPTER 5 CONCLUSION

5.1 Summary of Results

In Chapter 2, A LMMSE prediction-based power-control algorithm was developed for a wireless CDMA-based multiple cellular networked system despite uncertain multipath fading. The predictor uses local SINR measurements at the previous and current time instances, along with the Doppler frequency (which can also be estimated from the SINR measurements) to estimate the channel uncertainties. A Lyapunov-based analysis is used to develop the controller and a resulting ultimate bound for the sampled SINR error, which can be decreased up to a point by increasing the control gains. Simulations indicate that the SINRs of all the radio links are regulated in the region $\gamma_{\min} \leq x_i(\cdot) \leq \gamma_{\max}$ with an outage probability of less than 10%, and power requirements of all the MTs were in the implementable range. Outages at some samples were determined to be due to limitations of the linear predictor, and this highlights the need for more sophisticated prediction and control development tools to address this issue. Simulations are also done using 2-bit and 3-bit control feedback, and the results show that the performance is still within the acceptable outage range if at least a 3-bit power control command is used. Comparison against a standard power control algorithm from the literature is done to demonstrate the advantages of using channel prediction and multi-bit feedback.

In Chapter 3, a model for collisions is developed and incorporated in the continuous CSMA Markov chain. An online distributed algorithm for maximizing the collision-free transmission states is developed that estimates the rates from the steady-state distribution of the Markov states. To account for the rate constraints, a constrained optimization problem is defined, and a numerical solution is suggested. Simulation results infer that the average number of collisions by using the optimized parameters is reduced to less than 0.2%. In addition, a model for collisions caused due to hidden terminals is developed and incorporated in the continuous CSMA Markov chain. A constrained optimization

problem is defined, and a numerical solution is suggested. Simulation results are provided to demonstrate the stability of the queues for a given stable set of arrival rates

In Chapter 4, a continuous control strategy is suggested for a DiffServ network to track the desired ensemble average queue length level specified by the network operator. A Lyapunov-based stability analysis is provided to illustrate global asymptotic tracking of the queue lengths in the Premium Service buffer. In addition, arrival rate delays due to propagation and processing that affects the control input of the Ordinary Service buffer is addressed, and a Lyapunov-based stability analysis is provided to illustrate global asymptotic tracking of the ensemble average queue length of this service. Simulations demonstrate the performance and feasibility of the controller, along with showing global asymptotic tracking of the queue lengths in the Premium Service and Ordinary Service buffers.

5.2 Recommendations for Future Work

Future efforts will focus extending the result in Chapter 3 to design cross-layer throughput maximization and topology reconfiguration algorithms to address mobility, energy, and queue length constraints at the terminals. Further, service rate limitations in Chapter 4 remains an open problem that could be further explored.

APPENDIX A
ESTIMATION OF RANDOM PROCESSES

A-1 General MMSE based estimation theory

Let $W(l)$ be some random process that needs to be estimated. The problem of finding the estimates of the zero mean gaussian random variables can be defined as

$$\begin{aligned}\varepsilon_{\min}^2 &= \min_{\hat{W}(l)} E \left[\left(W(l) - \hat{W}(l) \right)^2 \right] \text{ given } W(l-1), W(l-2), W(l-3), \dots \\ &= \min_{\hat{W}(l)} E \left[\left(W^2(l) - 2\hat{W}(l)W(l) + \hat{W}^2(l) \right) \right] \text{ given } W(l-1), W(l-2), W(l-3), \dots \\ &= \min_{\hat{W}(l)} E \left[W^2(l) \right] - 2\hat{W}(l)E \left[W(l) \right] + \hat{W}^2(l) \text{ given } W(l-1), W(l-2), W(l-3), \dots\end{aligned}$$

To find the minimum value of the estimate of W ,

$$\begin{aligned}\frac{d}{d\hat{W}(l)} \left\{ E \left[W^2(l) \right] - 2\hat{W}(l)E \left[W(l) \right] \right\} &= 0 \text{ given } W(l-1), W(l-2), W(l-3), \dots \\ \implies 0 - 2E \left[W(l) \right] + 2\hat{W}(l) &= 0 \text{ given } W(l-1), W(l-2), W(l-3), \dots\end{aligned}$$

The estimate is given [65] as

$$\hat{W}(l) = E \left[W(l) \mid W(l-1), W(l-2), W(l-3), \dots \right].$$

The conditional estimate is given by

$$E \left[W(l) \mid W(l-1), W(l-2), W(l-3), \dots \right],$$

where $W(l), W(l-1), W(l-2), W(l-3), \dots$ are all jointly gaussian and $W(l-1), W(l-2), W(l-3), \dots$ are the past values of the random variable W that are used to estimate the current value $W(l)$.

A-2 Gaussian Case

The conditional probability density function is given by [101]

$$\begin{aligned} & f_{W(l)} [W(l) | W(l-1), W(l-2), W(l-3), \dots] \\ &= \frac{f_{W(l), W(l-1), W(l-2), \dots} [W(l), W(l-1), W(l-2), W(l-3), \dots]}{f_{W(l-1), W(l-2), \dots} [W(l-1), W(l-2), W(l-3), \dots]}, \end{aligned}$$

where the numerator and denominator are joint density functions of the zero-mean gaussian random variables W upto instants l and $l-1$ respectively. The Covariance Matrices K_n and K_{n-1} are defined as

$$\begin{aligned} K_n &= E [Y_l \cdot Y_l^T], \\ \text{and } K_{n-1} &= E [Y_{l-1} \cdot Y_{l-1}^T], \end{aligned}$$

where

$$\begin{aligned} Y_l &= \begin{bmatrix} W(l-s) & W(l-(s-1)) & \dots & W(l) \end{bmatrix}^T, \\ \text{and } Y_{l-1} &= \begin{bmatrix} W(l-s) & W(l-(s-1)) & \dots & W(l-1) \end{bmatrix}^T. \end{aligned}$$

Since the means of the random variables W are zero at any l

$$\begin{aligned} & f_{W(l)} [W(l) | W(l-1), W(l-2), W(l-3), \dots] \\ &= \frac{\exp \left\{ -\frac{1}{2} Y_l^T K_n^{-1} Y_l \right\}}{(2\pi)^{\frac{n}{2}} |K_n|^{1/2}} \cdot \left\{ \frac{\exp \left\{ -\frac{1}{2} Y_{l-1}^T K_{n-1}^{-1} Y_{l-1} \right\}}{(2\pi)^{\frac{(n-1)}{2}} |K_{n-1}|^{1/2}} \right\}^{-1}. \end{aligned} \quad (\text{A-1})$$

Since $W(l)$ is a zero-mean gaussian random process, the MMSE estimate is a linear estimate, i.e., $E [W(l) | W(l-1), W(l-2), W(l-3), \dots]$ can be obtained by manipulating Equation A-1. For a simple case with only one given value, the linear MMSE estimation is

given by

$$\begin{aligned} E [W(l) | W(l-1)] &= \mu_{W(l)} + \rho_{W(l)W(l-1)} \left(\frac{\sigma_{W(l)}}{\sigma_{W(l-1)}} \right) (W(l-1) - \mu_{W(l-1)}) \\ &= \left[\rho_{W(l)W(l-1)} \left(\frac{\sigma_{W(l)}}{\sigma_{W(l-1)}} \right) \right] W(l-1), \end{aligned} \tag{A-2}$$

where $\rho_{W(l)W(l-1)}$ is the autocorrelation function, $\sigma_{W(l)}$ and $\sigma_{W(l-1)}$ are the variances.

APPENDIX B
ORTHOGONALITY CONDITION

Let $Y, X_1, X_2, X_3, \dots, X_N$ be gaussian random variables with zero means. The MMSE estimate is the conditional mean, given by

$$E[Y | X_1, X_2, X_3, \dots, X_N] = \sum_{k=1}^N a_k X_k.$$

The random variables $\left(Y - \sum_{k=1}^N a_k X_k\right), X_1, X_2, X_3, \dots, X_N$ are jointly gaussian. Since the first term is uncorrelated with all the rest, it can be inferred that the random variable $\left(Y - \sum_{k=1}^N a_k X_k\right)$ is uncorrelated with $X_1, X_2, X_3, \dots, X_N$. Therefore,

$$\begin{aligned} E \left[\left(Y - \sum_{k=1}^N a_k X_k \right) | X_1, X_2, X_3, \dots, X_N \right] &= E \left[\left(Y - \sum_{k=1}^N a_k X_k \right) \right] \\ &= E[Y] - \sum_{k=1}^N a_k E[X_k] = 0, \end{aligned}$$

since $E[Y] = E[X_k] = 0$. The condition

$$E \left[\left(Y - \sum_{k=1}^N a_k X_k \right) | X_1, X_2, X_3, \dots, X_N \right] = 0 \quad (\text{B-1})$$

is known as the *Orthogonality Condition*, which can also be written as

$$[Y - a^T X] \perp X,$$

where

$$X = \begin{bmatrix} X_1 & X_2 & \dots & X_N \end{bmatrix}^T.$$

The a_i 's can be obtained from the orthogonality condition.

Note: From Equation B-1, we get

$$E[Y | X_1, X_2, X_3, \dots, X_N] - \sum_{k=1}^N a_k E[X_k | X] = 0.$$

$$\begin{aligned} \implies E[Y | X_1, X_2, X_3, \dots, X_N] - \sum_{k=1}^N a_k X_k &= 0 \\ \implies E[Y | X_1, X_2, X_3, \dots, X_N] &= \sum_{k=1}^N a_k X_k. \end{aligned}$$

Thus, the conditional mean of a zero-mean gaussian random variable Y is given by a linear estimate of the given variables X_i s.

Calculation of a_i 's.

From the Orthogonality condition in Equation B-1 [65]

$$\begin{aligned} E \left[\left(Y - \sum_{k=1}^N a_k X_k \right) | X_p \right] &= 0, \quad 1 \leq p \leq N \\ \implies E[Y X_p] &= \sum_{k=1}^N a_k E[X_k X_p], \quad 1 \leq p \leq N. \\ \implies k_{YX} &= a^T K_{XX}, \end{aligned} \tag{B-2}$$

where

$$\begin{aligned} a &\triangleq \begin{bmatrix} a_1 & a_2 & \dots & a_N \end{bmatrix}^T, \\ k_{YX} &\triangleq \begin{bmatrix} E[Y X_1] & E[Y X_2] & E[Y X_3] & \dots & E[Y X_N] \\ K_{YX_1} & K_{YX_2} & K_{YX_3} & \dots & K_{YX_N} \end{bmatrix}, \end{aligned}$$

and the covariance matrix

$$K_{XX} = E[XX^T].$$

From Equation B-2

$$a^T = k_{YX} K_{XX}^{-1}.$$

APPENDIX C
PROOF OF $P \geq 0$

Lemma: The solution to the differential equation

$$\dot{P}(t) = -r_p \left(\dot{\lambda}_p^a - \beta \operatorname{sgn}(e_p) \right), \quad (\text{B-1})$$

$$P(e_p(t_0), t_0) = \beta |e_p(0)| - e_p(0) \dot{\lambda}_p(0) \quad (\text{B-2})$$

satisfies the condition

$$P(e_p, t) \geq 0$$

if β satisfies the condition

$$\beta > \zeta_{\dot{\lambda}_p^a} + \frac{1}{\alpha_p} \zeta_{\ddot{\lambda}_p^a}. \quad (\text{B-3})$$

Proof. By using (4–5), integrating by parts, and regrouping yields

$$\begin{aligned} & \int_0^t r_p \left(\dot{\lambda}_p^a(\tau) - \beta \operatorname{sgn}(e_p(\tau)) \right) d\tau = \int_0^t \dot{e}_p \left(\dot{\lambda}_p^a(\tau) - \beta \operatorname{sgn}(e_p(\tau)) \right) d\tau \\ & + \int_0^t \alpha_p e_p \left(\dot{\lambda}_p^a(\tau) - \beta \operatorname{sgn}(e_p(\tau)) \right) d\tau \\ = & \dot{\lambda}_p^a(t) e_p(t) - \dot{\lambda}_p^a(0) e_p(0) - \beta |e_p(t)| + \beta |e_p(0)| \\ & - \int_0^t \alpha_p e_p \left(\frac{1}{\alpha_p} \frac{\partial \dot{\lambda}_p^a(\tau)}{\partial \tau} \right) d\tau + \int_0^t \alpha_p e_p \left(\dot{\lambda}_p^a(\tau) - \beta \operatorname{sgn}(e_p(\tau)) \right) d\tau. \end{aligned} \quad (\text{B-4})$$

From (2–13), the expression in (B-4) can be upper bounded by

$$\begin{aligned} & \int_0^t r_p \left(\dot{\lambda}_p(\tau) - \beta \operatorname{sgn}(e_p(\tau)) \right) d\tau \leq |e_p(t)| \left[\zeta_{\dot{\lambda}_p} - \beta \right] \\ & + \beta |e_p(0)| - \dot{\lambda}_p(0) e_p(0) + \int_0^t \alpha_p |e_p(\tau)| \left(\zeta_{\dot{\lambda}_p^a} + \frac{1}{\alpha_p} \zeta_{\ddot{\lambda}_p^a} - \beta \right) d\tau. \end{aligned}$$

Therefore, if the condition in (B-3) is satisfied, then

$$\begin{aligned}
& \int_0^t r_p \left(\dot{\lambda}_p^a(\tau) - \beta \operatorname{sgn}(e_p(\tau)) \right) d\tau \\
& \leq \beta |e_p(0)| - \dot{\lambda}_p^a(0) e_p(0) \\
& \leq P(e_p(t_0), t_0).
\end{aligned} \tag{B-5}$$

Integrating (B-1) on both sides, and using (B-2) yields

$$\begin{aligned}
P(e_p(t), t) &= \beta |e_p(0)| - e_p(0) \dot{\lambda}_p^a(0) \\
&\quad - \int_0^t r_p(\tau) \left(\dot{\lambda}_p^a(\tau) - \beta \operatorname{sgn}(e_p(\tau)) \right) d\tau,
\end{aligned}$$

which indicates that $P(e_p(t), t) \geq 0$ from (B-5). □

REFERENCES

- [1] J. Aein, "Power balancing in systems employing frequency reuse," *COMSAT Tech. Rev.*, pp. 277–299, 1973.
- [2] H. Alavi and R. W. Nettleton, "Downstream power control for a spread spectrum cellular mobile radio system," in *Proc. IEEE Glob. Telecommun. Conf.*, 1982, pp. 84–88.
- [3] J. Zander., "Optimum global transmitter power control in cellular radio systems," in *Proc. IEEE Int. Symp. Personal Indoor Mob. Radio Commun.*, London, U.K., 1991.
- [4] —, "Distributed cochannel interference control in cellular radio systems," *IEEE Trans. Veh. Technol.*, vol. 41, pp. 305–311, 1992.
- [5] J. Zander, "Performance of optimum transmitter power control in cellular radio systems," *IEEE Trans. Veh. Technol.*, vol. 41, pp. 57–62, 1992.
- [6] G. Foschini and M. Z., "A simple distributed autonomous power control algorithm and its convergence," *IEEE Trans. Veh. Technol.*, vol. 42, pp. 641–646, 1993.
- [7] S. Grandhi and J. Zander, "Constrained power control in cellular radio systems," in *Proc. IEEE Veh. Technol. Conf.*, 8-10 Jun. 1994, pp. 824–828.
- [8] R. D. Yates, "A framework for uplink power control in cellular radio systems," *IEEE J. Sel. Area. Comm.*, vol. 13, pp. 1341–1347, Sep. 1995.
- [9] R. D. Yates and C. Y. Huang, "Integrated power control and base station assignment," *IEEE Trans. Veh. Technol.*, vol. 44, pp. 638–644, Aug. 1995.
- [10] R. Jantti and S.-L. Kim, "Second-order power control with asymptotically fast convergence," *IEEE J. Sel. Area. Comm.*, vol. 18, no. 3, pp. 447–457, 2000.
- [11] N. Bambos, S. Chen, and G. Pottie, "Channel access algorithms with active link protection for wireless communication networks with power control," *IEEE/ACM Trans. Netw.*, vol. 8, no. 5, pp. 583–597, 2000.
- [12] T. Alpcan, X. Fan, T. Basar, M. Arcak, and J. Wen, "Power control for multicell CDMA wireless networks: a team optimization approach," in *Int. Symp. Model. Optim. Mob. Ad Hoc Wireless Netw.*, 3-7 Apr. 2005, pp. 379–388.
- [13] S. Dontula and S. Jagannathan, "Active link protection for wireless peer-to-peer and cellular networks with power control," in *World Wireless Congr.*, 2004, pp. 612–617.
- [14] S. Ariyavisitakul, "SIR-based power control in a CDMA system," in *Proc. IEEE Glob. Telecommun. Conf.*, 6–9 Dec. 1992, pp. 868–873.

- [15] S. Kandukuri and S. Boyd, “Optimal power control in interference-limited fading wireless channels with outage-probability specifications,” *IEEE Trans. Wireless Commun.*, vol. 1, no. 1, pp. 46–55, Jan. 2002.
- [16] K.-L. Hsiung, S.-J. Kim, and S. Boyd, “Power control in lognormal fading wireless channels with uptime probability specifications via robust geometric programming,” in *Proc. American Control Conf.*, Portland, OR, Jun. 2005, pp. 3955–3959.
- [17] K. Yang, Y. Wu, J. Huang, X. Wang, and S. Verdu, “Distributed robust optimization for communication networks,” in *Proc. IEEE INFOCOM*, Apr. 2008, pp. 1157–1165.
- [18] C. W. Tan, D. Palomar, and M. Chiang, “Energy–robustness tradeoff in cellular network power control,” *IEEE/ACM Trans. Networking*, vol. 17, no. 3, pp. 912–925, June 2009.
- [19] C. W. Tan, “Optimal power control in rayleigh-fading heterogeneous networks,” in *Proc. 2011 IEEE INFOCOM*, Apr. 2011, pp. 2552–2560.
- [20] S. Jagannathan, M. Zawodniok, and Q. Shang, “Distributed power control for cellular networks in the presence of channel uncertainties,” *IEEE Trans. Wireless Commun.*, vol. 5, no. 3, 2006.
- [21] M. Rintamaki, H. Koivo, and I. Hartimo, “Adaptive closed-loop power control algorithms for CDMA cellular communication systems,” *IEEE Trans. Veh. Technol.*, vol. 53, no. 6, pp. 1756–1768, Nov. 2004.
- [22] —, “Application of the generalized predictive control method in closed-loop power control of CDMA cellular communication systems,” in *Proc. 6th Nordic Signal Process. Symposium*, 2004, pp. 252–255.
- [23] J.-H. Wen, J. Y. Wang, and T. K. Woo, “Distributed power balancing with linear prediction and adaptive on-off strategies for CDMA cellular mobile systems,” *Wireless Pers. Commun.*, vol. 21, pp. 229–244, 2002.
- [24] J.-H. Wen, L. Yeh, and J. Chiou, “Performance of short-term fading prediction-based power control method for DS-CDMA cellular mobile radio networks,” *IEICE Trans. Commun.*, vol. E81-B, no. 3, pp. 1231–1238, 1998.
- [25] J.-H. Wen and S. Y. Lin, “An uplink short-term fading prediction-based power control method for DS-CDMA cellular radio systems,” *Wireless Pers. Commun.*, vol. 15, pp. 221–237, 2000.
- [26] T. Eyceoz, A. Duel-Hallen, and H. Hallen, “Deterministic channel modeling and long range prediction of fast fading mobile radio channels,” *IEEE Commun. Lett.*, vol. 2, no. 9, pp. 254–256, Sept. 1998.

- [27] S. Hu, H. Hallen, and A. Duel-Hallen, “Physical channel modeling, adaptive prediction and transmitter diversity for flat fading mobile channel,” in *IEEE Workshop Signal Process. Adv. Wireless Commun.*, 9-12 May 1999, pp. 387–390.
- [28] A. Duel-Hallen, S. Hu, and H. Hallen, “Long range prediction of fading signals: Enabling adaptive transmission for mobile radio channels,” *IEEE Signal. Proc. Mag.*, vol. 17, no. 3, pp. 62–75, May 2000.
- [29] S. Subramanian, J. Shea, and W. E. Dixon, “Prediction-based power control for distributed cellular communication networks with time-varying channel uncertainties,” in *Proc. IEEE Conf. Decis. Control*, Shanghai, China, 2009, pp. 1998–2003.
- [30] L. Song, N. B. Mandayam, and Z. Gajic, “Analysis of an up/down power control algorithm for the CDMA reverse link under fading,” *IEEE J. Select. Commun.*, vol. 19, no. 2, pp. 277–286, 2001.
- [31] R. Boorstyn, A. Kershenbaum, B. Maglaris, and V. Sahin, “Throughput analysis in multihop CSMA packet radio networks,” *IEEE Trans. Commun.*, vol. 35, no. 3, pp. 267–274, Mar. 1987.
- [32] X. Wang and K. Kar, “Throughput modelling and fairness issues in CSMA/CA based ad-hoc networks,” in *Proc. IEEE Annu. Joint Conf. IEEE Comput. and Commun. Societies INFOCOM 2005*, vol. 1, 2005, pp. 23–34.
- [33] L. Jiang and J. Walrand, “A distributed CSMA algorithm for throughput and utility maximization in wireless networks,” *IEEE/ACM Trans. Netw.*, vol. 18, no. 3, pp. 960–972, 2010.
- [34] G. Bianchi, “Performance analysis of the IEEE 802.11 distributed coordination function,” *IEEE J. Select. Commun.*, vol. 18, no. 3, pp. 535–547, Mar. 2000.
- [35] —, “IEEE 802.11—Saturation throughput analysis,” *IEEE Commun. Lett.*, vol. 2, no. 12, pp. 318–320, Dec. 1998.
- [36] P. Marbach, A. Eryilmaz, and A. Ozdaglar, “Achievable rate region of CSMA schedulers in wireless networks with primary interference constraints,” in *Proc. IEEE Conf. Decis. Control*, 2007, pp. 1156–1161.
- [37] L. Jiang and J. Walrand, “Approaching throughput-optimality in distributed CSMA scheduling algorithms with collisions,” *IEEE/ACM Trans. Netw.*, vol. 19, no. 3, pp. 816–829, 2011.
- [38] F. P. Kelly, A. Maulloo, and D. Tan, “Rate control in communication networks: shadow prices, proportional fairness and stability,” *J. Oper. Res. Soc.*, vol. 49, pp. 237–252, 1998.
- [39] S. Liu, T. Basar, and R. Srikant, “Controlling the internet: A survey and some new results,” in *IEEE Conf. Decision and Control*, vol. 3, 2003, pp. 3048–3057.

- [40] —, “Exponential-RED: A stabilizing AQM scheme for low- and high-speed TCP protocols,” *IEEE/ACM Trans. Netw.*, vol. 13, no. 5, pp. 1068–1081, 2005.
- [41] D. Tipper and M. K. Sundareshan, “Numerical methods for modeling computer networks under nonstationary conditions,” *IEEE J. Select. Commun.*, vol. 8, no. 9, pp. 1682–1695, 1990.
- [42] R. Braden, D. Clark, and S. Shenker, “Integrated services in the Internet architecture: An overview,” Tech. Rep., Jun. 1994, network Working Group, RFC 1633.
- [43] D. Black, S. Blake, M. Carlson, E. Davies, Z. Wang, and W. Weiss, “An architecture for Differentiated Services,” Tech. Rep., June 1994, network Working Group, RFC 2475.
- [44] C. Agnew, “Dynamic modeling and control of congestion-prone systems,” *Oper. Res.*, vol. 24, no. 3, pp. 400–419, 1976.
- [45] C. E. Rohrs, R. A. Berry, and S. J. O’Halek, “A control engineer’s look at ATM congestion avoidance,” in *Proc. IEEE Global Telecomm.*, vol. 2, 1995, pp. 1089–1094.
- [46] A. Segall, “The modeling of adaptive routing in data communication networks,” *IEEE Trans. Commun.*, vol. 25, no. 1, pp. 85–95, 1977.
- [47] S. Keshav, “A control-theoretic approach to flow control,” *SIGCOMM Comput. Commun. Rev.*, vol. 25, no. 1, pp. 188–201, Jan. 1995.
- [48] L. Benmohamed and S. M. Meerkov, “Feedback control of congestion in packet switching networks: the case of a single congested node,” *IEEE/ACM Trans. Netw.*, vol. 1, no. 6, pp. 693–708, 1993.
- [49] L. Benmohamed and Y. T. Wang, “A control-theoretic ABR explicit rate algorithm for ATM switches with per-VC queueing,” in *Proc. IEEE INFOCOM*, vol. 1, 1998, pp. 183–191.
- [50] A. Kolarov and G. Ramamurthy, “A control-theoretic approach to the design of an explicit rate controller for ABR service,” *IEEE/ACM Trans. Netw.*, vol. 7, no. 5, pp. 741–753, 1999.
- [51] A. Pitsillides and J. Lambert, “Adaptive congestion control in ATM based networks: quality of service with high utilisation,” *J. Comput. Commun.*, vol. 20, pp. 1239–1258, 1997.
- [52] A. Pitsillides, Y. A. Sekercioglu, and G. Ramamurthy, “Effective control of traffic flow in atm networks using fuzzy explicit rate marking (ferm),” *IEEE J. Sel. Areas Commun.*, vol. 15, no. 2, pp. 209–225, 1997.

- [53] A. Pitsillides and P. Ioannou, "Combined nonlinear control of flow rate and bandwidth for virtual paths in atm based networks," in *IEEE Mediterranean Symp. New Directions in Control and Automation*, July 11-13 1995, pp. 177–184.
- [54] A. Pitsillides, P. Ioannou, and D. Tipper, "Integrated control of connection admission, flow rate, and bandwidth for ATM based networks," in *Proc. IEEE INFOCOM*, vol. 2, 1996, pp. 785–793.
- [55] Y. A. Sekercioglu, A. Pitsillides, and P. Ioannou, "A simulation study on the performance of integrated switching strategy for traffic management in ATM networks," in *Proc. IEEE Symp. Comput. and Commun.*, 1998, pp. 13–18.
- [56] A. Pitsillides, P. Ioannou, M. Lestas, and L. Rossides, "Adaptive nonlinear congestion controller for a differentiated-services framework," *IEEE/ACM Trans. Netw.*, vol. 13, no. 1, pp. 94–107, 2005.
- [57] K. Bouyoucef and K. Khorasani, "A robust distributed congestion-control strategy for differentiated-services network," *IEEE Trans. Ind. Electron.*, vol. 56, no. 3, pp. 608–617, 2009.
- [58] N. Zhang, M. Yang, Y. Jing, and S. Zhang, "Congestion control for DiffServ network using second-order sliding mode control," *IEEE Trans. Ind. Electron.*, vol. 56, no. 9, pp. 3330–3336, 2009.
- [59] C. Makkar, G. Hu, W. G. Sawyer, and W. E. Dixon, "Lyapunov-based tracking control in the presence of uncertain nonlinear parameterizable friction," *IEEE Trans. Automat. Control*, vol. 52, pp. 1988–1994, 2007.
- [60] P. M. Patre, W. Mackunis, C. Makkar, and W. E. Dixon, "Asymptotic tracking for systems with structured and unstructured uncertainties," *IEEE Trans. Control Syst. Technol.*, vol. 16, pp. 373–379, 2008.
- [61] A. J. Viterbi, *CDMA: Principles of Spread Spectrum Communication*. Addison Wesley, 1995.
- [62] R. Canchi and Y. Akaiwa, "Performance of adaptive transmit power control in $\pi/4$ DQPSK mobile radio systems in flat Rayleigh fading channels," in *Proc. IEEE Veh. Technol. Conf.*, vol. 2, 16-20 May 1999, pp. 1261–1265vol.2.
- [63] T. Rappaport, *Wireless Communications, Principles and Practice*. Prentice Hall, 1999.
- [64] L. Gao and T. Wong, "Power control and spreading sequence allocation in a CDMA forward link," *IEEE Trans. Inf. Theory*, vol. 50, no. 1, pp. 105–124, Jan. 2004.
- [65] H. Stark and J. Woods, *Probability and Random Processes with Applications to Signal Processing*, 3rd ed. Prentice Hall, 2002.

- [66] L. Krasny, H. Arslan, D. Koilpillai, and S. Chennakeshu, “Doppler spread estimation in mobile radio systems,” *IEEE Comm. Lett.*, vol. 5, no. 5, pp. 197–199, May 2001.
- [67] L. Qian and Z. Gajic, “Variance minimization stochastic power control in cdma systems,” *IEEE Trans. Wireless Commun.*, vol. 5, no. 1, pp. 193–202, 2006.
- [68] R. H. Clarke, “A statistical theory of mobile-radio reception,” *Bell Sys. Tech. J.*, vol. 47, no. 6, pp. 957–1000, Jul.–Aug. 1968.
- [69] W. C. Jakes, *Microwave Mobile Communications*. Wiley, 1974.
- [70] S. Subramanian, J. Shea, and W. E. Dixon, “Power control for cellular communications with channel uncertainties,” in *Proc. Am. Control Conf.*, St. Louis, Missouri, June 2009, pp. 1569–1574.
- [71] J. Spooner, M. Maggiore, R. Ordonez, and K. Passino, *Stable Adaptive Control and Estimation for Nonlinear Systems*. Wiley, 2002.
- [72] S. PalChaudhuri, J.-Y. Le Boudec, and M. Vojnovic, “Perfect simulations for random trip mobility models,” in *Proc. Annu. Simul. Symp.*, 4-6 Apr. 2005, pp. 72–79.
- [73] J.-Y. Le Boudec and M. Vojnovic, “Perfect simulation and stationarity of a class of mobility models,” in *Proc. IEEE Int. Conf. Comput. Commun.*, vol. 4, 13-17 Mar. 2005, pp. 2743–2754vol.4.
- [74] L. Devroye, *Non-Uniform Random Variate Generation*. Springer-Verlag, 1986.
- [75] J. Papandriopoulos, J. Evans, and S. Dey, “Optimal power control for Rayleigh-faded multiuser systems with outage constraints,” *IEEE Trans. Wireless Commun.*, vol. 4, no. 6, pp. 2705–2715, November 2005.
- [76] M. Suzuki and H. Sasaoka, “Performance of orthogonal TPC-CDMA cellular system using cell configuration strategy,” in *Proc. Vehicle Navigation and Information Systems Conf.*, 1994, pp. 181–186.
- [77] C.-J. Chang, J.-H. Lee, and F.-C. Ren, “Design of power control mechanisms with PCM realization for the uplink of a DS-CDMA cellular mobile radio system,” *IEEE Trans. Veh. Technol.*, vol. 45, no. 3, pp. 522–530, Aug. 1996.
- [78] K. P. Kelly, *Reversibility and Stochastic Networks*. Wiley, 1979.
- [79] S. Boyd and L. Vandenberghe, *Convex Optimization*. New York, NY, USA: Cambridge University Press, 2004.
- [80] D. P. Bertsekas, *Nonlinear Programming*. Belmont, MA: Athena Scientific, 1999.
- [81] D. G. Luenberger, *Introduction to Linear and Nonlinear Programming*. Addison-Wesley, 1973.

- [82] M. S. Bazaraa, H. D. Sherali, and C. M. Shetty, *Nonlinear programming - Theory and algorithms (2nd Edition)*. Wiley, 1993.
- [83] R. H. Byrd and J. C. Gilbert, “A trust region method based on interior point techniques for nonlinear programming,” *Mathematical Programming*, vol. 89, pp. 149–185, 1996.
- [84] R. H. Byrd, M. E. H. Y, and J. N. Z, “An interior point algorithm for large scale nonlinear programming,” *SIAM J. Optim.*, 1999.
- [85] J. Filipiak, *Modelling and control of dynamic flows in communication networks*, ser. Communications and control engineering series. Springer, 1988.
- [86] S. Sharma and D. Tipper, “Approximate models for the study of nonstationary queues and their applications to communication networks,” in *Proc. IEEE Int. Commun. Conf.*, vol. 1, 1993, pp. 352–358.
- [87] X. Gu, K. Sohrawy, and D. R. Vaman, *Control And Performance In Packet, Circuit, And ATM Networks*. Norwell, MA: Kluwer Academic Pub, 1995.
- [88] K. Bouyoucef and K. Khorasani, “Robust feedback linearization-based congestion control using a fluid flow model,” in *Proc. Am. Control Conf.*, Jun. 2006, pp. 4882–4887.
- [89] —, “A robust congestion control strategy for delay dependent differentiated-services networks,” in *Proc. IEEE Int. Symp. Ind. Electron.*, 2007, pp. 2905–2910.
- [90] —, “A sliding mode-based congestion control for time delayed differentiated-services networks,” in *Proc. Med. Conf. Cont. Aut.*, Jun. 2007, pp. 1–6.
- [91] A. Filippov, “Differential equations with discontinuous right-hand side,” *Am. Math. Soc. Transl.*, vol. 42 no. 2, pp. 199–231, 1964.
- [92] A. F. Filippov, *Differential Equations with Discontinuous Right-hand Sides*. Kluwer Academic Publishers, 1988.
- [93] G. V. Smirnov, *Introduction to the theory of differential inclusions*. American Mathematical Society, 2002.
- [94] J. P. Aubin and H. Frankowska, *Set-valued analysis*. Birkhuser, 2008.
- [95] F. H. Clarke, *Optimization and nonsmooth analysis*. SIAM, 1990.
- [96] B. Paden and S. Sastry, “A calculus for computing Filippov’s differential inclusion with application to the variable structure control of robot manipulators,” *IEEE Trans. Circuits Syst.*, vol. 34 no. 1, pp. 73–82, 1987.
- [97] D. Shevitz and B. Paden, “Lyapunov stability theory of nonsmooth systems,” *IEEE Trans. Autom. Control*, vol. 39 no. 9, pp. 1910–1914, 1994.

- [98] R. Leine and N. van de Wouw, “Non-smooth dynamical systems,” in *Stability and Convergence of Mechanical Systems with Unilateral Constraints*, ser. Lecture Notes in Applied and Computational Mechanics. Springer Berlin / Heidelberg, 2008, vol. 36, pp. 59–77.
- [99] H. K. Khalil, *Nonlinear Systems*, 3rd ed. Prentice Hall, 2002.
- [100] S. Subramanian, J. W. Curtis, E. L. Pasiliao, J. M. Shea, and W. E. Dixon, “Continuous congestion control for differentiated-services networks,” in *Proc. IEEE Conf. Decis. Control*, Maui, HI, Dec. 2012.
- [101] A. Leon-Garcia, *Probability and Random Processes for Electrical Engineering*, 2nd ed. Addison Wesley, 1994.

BIOGRAPHICAL SKETCH

Sankrith Subramanian was born in Chennai, India in 1985. He received his Bachelor of Engineering degree in instrumentation and control engineering from St. Joseph's College of Engineering (Anna University), India, in 2006, and his Master of Science degree in electrical and computer engineering from the University of Florida in 2009. His interests lie in the field of networked control systems and cross-layer design.

Sankrith pursued his Doctor of Philosophy in the Department of Electrical and Computer Engineering. He was a Graduate Research Assistant in the Nonlinear Controls and Robotics group at the University of Florida, under the supervision of Dr. Warren E. Dixon. He was co-advised by Dr. John M. Shea of the Wireless Information Networking Group at the University of Florida. He was also collaborating with Air Force Research Laboratory, Eglin Air Force Base, Florida, while working towards his PhD.

The primary focus of his research was to address the challenges faced in various layers of dynamic communication networks, and design control algorithms and cross layer schemes.